Missouri S&T Library and Learning Resources

Scholars' Mine

Doctoral Dissertations | Student Theses and Dissertations

Fall 2020

Structured catalysts designed and manufactured by 3D-printing technique for functional integration of catalytic systems

Fatima Magzoub

Follow this and additional works at: https://scholarsmine.mst.edu/doctoral_dissertations

 Part of the Chemical Engineering Commons

Department: Chemical and Biochemical Engineering

Recommended Citation

Magzoub, Fatima, "Structured catalysts designed and manufactured by 3D-printing technique for functional integration of catalytic systems" (2020). *Doctoral Dissertations*. 3077.
https://scholarsmine.mst.edu/doctoral_dissertations/3077

This thesis is brought to you by Scholars' Mine, a service of the Missouri S&T Library and Learning Resources. This work is protected by U. S. Copyright Law. Unauthorized use including reproduction for redistribution requires the permission of the copyright holder. For more information, please contact scholarsmine@mst.edu.

STRUCTURED CATALYSTS DESIGNED AND MANUFACTURED BY 3D-PRINTING TECHNIQUE FOR FUNCTIONAL INTEGRATION OF CATALYTIC SYSTEMS

by

FATIMA MAHGOUB MAGZOUB

A DISSERTATION

Presented to the Graduate Faculty of the

MISSOURI UNIVERSITY OF SCIENCE AND TECHNOLOGY

In Partial Fulfillment of the Requirements for the Degree

DOCTOR OF PHILOSOPHY

in

CHEMICAL ENGINEERING

2020

Approved by:

Dr. Ali Rownaghi, Advisor
Dr. Douglas Ludlow
Dr. Fateme Rezaei
Dr. Angela Lueking
Dr. Mehdi Ferdowsi

© 2020

FATIMA MAHGOUB MAGZOUB

All Rights Reserved

PUBLICATION DISSERTATION OPTION

This dissertation contains three articles formatted in the style used by the Missouri of Science and Technology:

Paper I, Pages 6-39, "3D-printed ZSM-5 monoliths with metal dopants for methanol conversion in the presence and absence of carbon dioxide" has been published in Applied Catalysis B: Environmental 245: 486–495, 2019

Paper II, Pages 40-61, "3D-printed HZSM-5 and 3D-HZM5@SAPO-34 structured monoliths with controlled acidity and porosity for conversion of methanol to dimethyl ether" has been published in Fuel, 280: 118628, 2020.

Paper III, Pages 62-86, "Design and synthesis of Ga, Zr, and V-doped 3D-printed ZSM-5 monolithic catalysts for selective formation of DME from methanol" has been submitted to Energy & Fuel.

ABSTRACT

Microporous zeolites are widely used as heterogeneous catalysts in a wide variety of chemical and petrochemical industries to produce value-added chemicals and fuels, owing to their large surface area, acid-base properties, high thermal stability, and excellent shape-selectivity.

The overall goal of this research was to shape engineer composite zeolites and fine-tune their physiochemical properties to improve the catalytic production of dimethyl ether (DME) and light olefins that are typically used as substitution to diesel fuel and polymer precursors, respectively. Specifically, HZSM-5 and silicalite-1 zeolites were formulated into monolithic contactors using 3D printing technique, followed by subsequent SAPO-34 crystals growth through a secondary hydrothermal method to produce zeolite composites of core-shell structure with controlled micro-meso-macro-porosity. Furthermore, the 3D-printed ZSM-5 monoliths were doped with various metals such as Cr, Ga, Cu, Y, Mo, and Zn to control their surface acidity, and used as heterogeneous catalysts in light olefins and DME production through methanol dehydration reaction.

Analysis of catalytic performance revealed enhancement in products yield and improvement in catalyst stability. Due to the synergistic integration of surface acidity and hierarchical porosity, high yield of light olefins (70%) and DME (80%), and excellent anti-coking stability were demonstrated.

ACKNOWLEDGMENTS

I would like to thank my academic advisor, Dr. Ali Rownaghi, for his instructions, guidance, support, patience, and urgency to overcome difficulties in my academic career. I appreciate the time he shared with me talking over the experimental results, the suggestion for me, and his financial supports in the research and academic conferences.

I am also grateful to the other committee members, including Dr. Douglas Ludlow, Dr. Angela Lueking, and Dr. Mehdi Ferdowsi to guide me on the right path and to scrutinize different aspects of the research, and Dr. Fateme Rezaei for her excellent and constructive suggestions and sharing her experimental instrument.

I would like to express my thanks to all my friends in the lab, including, but not limited to, Dr. Xin Li, Qasim Al-Naddaf, Busuyi Adebayo, and Shane Lawson, who helped me with the experiments.

My sincere gratitude is also given to my husband for his prayers, his everlasting love, his understanding, his accompanies, his supports, and his patience. And my special thanks to my sons for their love, kisses, and hugs to encourage me and support me. I am grateful to my parents and sisters and brothers for their supporting, emboldening, and inspiring me when I am away from my home country. I thank God for His grace, love, and blesses.

TABLE OF CONTENTS

Page

LIST OF ILLUSTRATIONS

SECTION Page

PAPER II

PAPER III

LIST OF TABLES

1. INTRODUCTION

1.1. ZEOLITE

Zeolites naturally are minerals with a hydrated aluminosilicate composite originally by SiO_4 and AlO_4-tetrahedral which have the structure of crystalline microporous materials with three-dimensional (3D) frameworks [1]. In the past 200 years, approximately 40 natural zeolites have been specified, while 150 zeolites and even more have been synthesized. the good catalytic properties of zeolites A, X, Y, and ZMS-5 (natural and artificial) beside their unique adsorption, ion-exchange [2], and molecular sieve made them the most familiar, popular, and diffuse [3].

In zeolite structure, each tetrahedron consists of an oxygen atom in the four corners which is responsible to form several framework structures and crystals; by linked to close tetrahedral unit and hence bonded together which is forms the channels and cages controlled by Water molecules and cations, such as calcium, sodium, potassium and magnesium [4]. The change in zeolite structure and framework comes from rearranged the Aluminum, silicon, and oxygen atoms as in Figure 1.1 [5]. To distinguish between the different type of zeolites frameworks and structures, 3 letter code assign as decided from the Structure Commission of IZA such as MFI CHA LTA and FAU. The multiple frameworks besides the various channel dimensions, pore sizes, and different morphology have helped zeolites to prevalence and dependence on it in several areas such as ion exchange [6], adsorption[7,8], gas separation [9], animal cares [10].

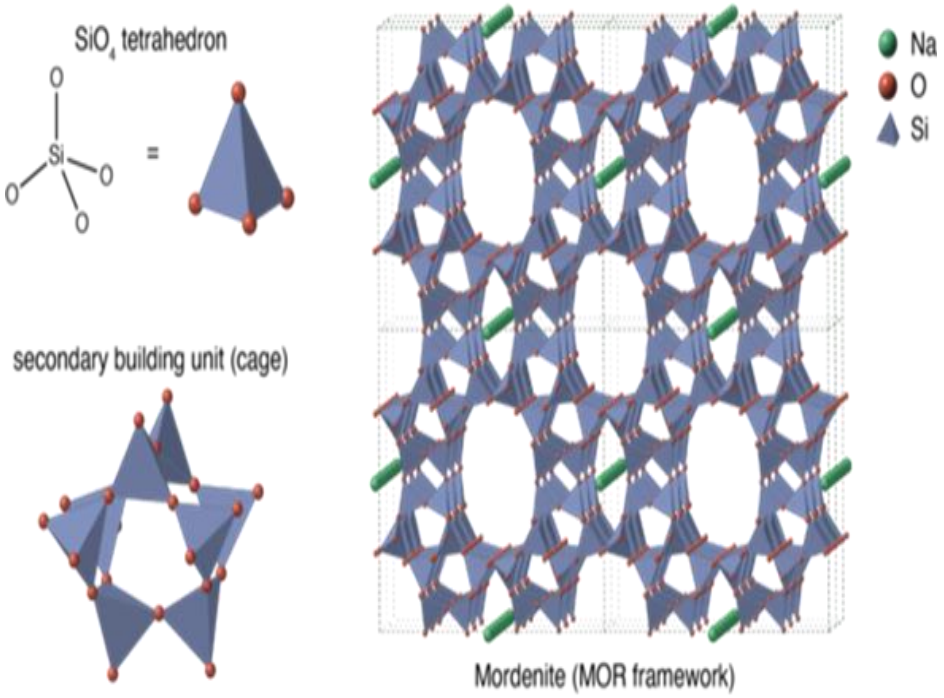

Figure 1. Schematic presentation of formation of zeolite framework.

1.2. METHANOL CONVERSION AND ZEOLITES

Since Zeolite Socony Mobil-5 (ZSM5) was developed in 1972 by a researcher in Mobil Oil Corporation and announced its neat properties represented in an exceptional structure and physical-chemical behave, shape selectivity, stability, and flexibility had become a high demand in many industrial processes[11]. A few years later methanol conversion to hydrocarbons through acidic zeolites as a catalytic process was patented [12]. Mainly, the methanol to hydrocarbons process consists of methanol to gasoline (MTG) which is no more environmentally eligible due to high aromatic contents, methanol to olefins (MTO), and MTD [13], methanol to aromatics (MTA) reaction [14], and methanol to olefins (MTO) reaction such as ethylene, propylene, butylene, and butadiene which is more industrial demand since proposed by Mobil Corporation in 1977, and is considered to be a correlation between the natural gas chemical industry and novel petrochemical industry[15,16]

Many zeolites reported and tested in methanol to hydrocarbons reaction such as ZSM5, silico-alumino-phosphate SAPO-34, and ZSM-22 [17,18]. Besides several studies controlled the deactivation of the catalysts via different preparation methods and structured technique [19].

1.3. METHANOL TO DIMETHYL EITHER (MTD)

MTD is one of the most significant technologies in the oil refinery industry, which produces an alternative clean fuel with environmentally properties which is DME[20].

Dimethyl ether (DME, CH_3OCH_3) is the simplest of the ethers made from methane and CO_2, which can be easily liquefied at 30°C and 6.06 bar and make it easy to transfer. While it has been counted as a clean fuel which could be a substitutional fuel for diesel engines. Besides the biodegradability properties and economic interests of the production [21]. Generally, DME can be produced in two ways, the indirect method including two steps for DME production by converting the Synthesis gas into methanol in the presence of a catalyst, followed by methanol dehydration in the presence of a different catalyst. or traditionally via the direct method consisting of one step for DME production by converting syngas-to-DME (STD) directly [22,23].

1.4. DESIGNED AND STRUCTURED ZEOLITE CATALYSTS

Several efforts have been made to design and structure the zeolites in many sides to upgrade the performance and improve the effectiveness as the catalysts. Some techniques were originated to promote the catalyst activity, rise the selectivity to the required product, and to progress catalyst stability and lifetime by optimizing the acidity,

adjusting the crystal size, changing the pore structure, and altering with heteroatoms. Herein we discuss the following novel approaches to design and structure zeolites to modify the porosity and acidity of the catalysts.

1.4.1. 3D-printing of Structured Catalysts. Rapid prototyping, or additive manufacturing, which is undergone by 3D printing has been a transformative technology in many fields, enabling structures with unique properties. The ability to 3D print catalyst structures will enable new functional catalytic materials that unite the appealing material properties of catalysts with tailored catalytic spices [24,25].

The 3D printing technique was used in many catalysts including zeolites, silicoaluminophosphate, aminosilica, and metal-organic frameworks, which is provided more stable structured catalysts for the reaction [24,26–31]. Therefore, it is reasonable to expect that using 3Dprinting to prepare catalytic materials will continue to develop in the coming years.

1.4.2. Modification with Metals. The literature represents two methods to modify the zeolite with metal, the impregnation methods, and ion exchange. Both methods are applied in the preparation of the catalysts and it improves interesting behavior and excellent selectivity [32,33]**.** In The ion exchange, the properties of zeolite such as porosity and acidity may be changed probably due to the replacement of zeolite cations with dispersed cations in the metal salt solution [34].

The modification of zeolite by impregnation method simply occurs when the zeolites impregnate the desired metal by nitrate or acetate aqueous solution. hence also the properties of the zeolite will be changed [35].

1.5. DISSERTATION OUTLINES

In Section 1 of this dissertation, three papers are represented. in Paper I, a brief introduction about Methanol dehydration and CO_2 co-feeding have been summarized over 3D-printed ZSM-5 monoliths doped with Ga_2O_3, Cr_2O_3, CuO, ZnO, MoO_3, and Y_2O_3 that were synthesized using the state-of-art 3D printing technique. Additionally, the factors, such as catalyst properties, reaction conditions, catalyst modification, and catalyst synthesis, which would be an important impact on Methanol dehydration were examined.

In Paper II, an additive manufacturing method was used for the rapid synthesis of HZSM- 5 structured monoliths (3D-HZSM5) with hierarchical porosity (macro-meso micro) and controlled the type and density of acid sites. It worth noting also 3D-HZSM5@SAPO-34 structured monolith was formed via the secondary growth method of silico-aluminophosphate (SAPO-34) on the 3D-HZSM5 monolith. The performance of the 3D-HZSM5 and 3D HZSM5@SAPO-34 structured monoliths were investigated in catalytic conversion of methanol to dimethyl ether (DME).

In Paper III, the facile and efficient method to design 3D-printed HZSM-5 modified with Ga, Zr, and v were presented. Results revealed that 4 %(Ga)/HZSM-5 zeolite monolith exhibits more stable activity in methanol dehydration and higher selectivity to DME than its powder counterpart. The coke formation has occurred at 400°C for all the monoliths.

In Section 2, the consequences of the dissertation works are abstracted, and the future work plans are determined.

PAPER

I. 3D-PRINTED ZSM-5 MONOLITHS WITH METAL DOPANTS FOR METHANOL CONVERSION IN THE PRESENCE AND ABSENCE OF CARBON DIOXIDE

Fatima Magzoub, Xin Li, Jawad Al-Darwish, Fateme Rezaei, Ali A. Rownaghi*
Department of Chemical and Biochemical Engineering, Missouri University of Science and Technology, 1101 N State St., Rolla, MO 65409, United States
*Fax: +1 573 341 4377; E-mail: rownaghia@mst.edu

ABSTRACT

The development of effective strategies to utilize CO_2 as a renewable feedstock for producing commercially viable products is an interesting challenge to explore new concepts and opportunities in catalysis and industrial chemistry. In this study, 3D-printed ZSM-5 monoliths doped with Ga_2O_3, Cr_2O_3, CuO, ZnO, MoO_3, and Y_2O_3were synthesized using the state-of-art 3D-printing technique. The physicochemical properties of the catalysts were characterized by X-ray diffraction, N_2 physisorption, NH_3 and CO_2 temperature-programed desorption and H_2 temperature-programmed reduction. The promotional effect of doped metals on catalytic performance of 3D-printed ZSM-5 monoliths in methanol to hydrocarbon (MTH) reaction in the presence and absence of CO_2 was investigated. Results indicated that both metal dopants type and reaction atmosphere greatly influence catalyst stability and product distribution. The yield of light olefins was enhanced over all metal-doped 3D-printed ZSM-5 monoliths in N_2 atmosphere (absence of CO_2), however, CO_2 atmosphere did not favor the production of light olefins. Although

selectivity toward ethylene slightly decreased, the propylene yield was almost constant after switching N_2 to CO_2 in MTH reaction at 400 °C. Furthermore, it was found that Y- and Zn-doped ZSM-5 monoliths exhibited higher yield of light olefins and BTX compounds in the in the absence and presence of CO_2, respectively.

Keywords: 3D-printing, ZSM-5 zeolite, Doped metals, CO_2 co-feeding, MTH reaction.

1. INTRODUCTION

The utilization of CO_2 as a sustainable carbon feedstock and soft oxidant for production of fuels and commercially value-added chemicals has drawn broad interests to the industrial chemistry (Al-Mamoori, Krishnamurthy, et al., 2017; He et al., 2016; Mondal et al., 2016; Zhu et al., 2011). Since CO_2 is a thermodynamically stable molecule, reactions of CO_2 must be combined with either high-energy reactants or use high temperature and pressure reaction conditions to gain a thermodynamic driving force. Several CO_2 utilization processes have been developed that lead to production of urea, methanol, and salicylic acid. Moreover, the promotional effects of CO_2 as a soft oxidant on alkane dehydrogenation (C–H bond scission) and cycloaddition over homogeneous and heterogeneous catalysts have been investigated in detail (Al-Mamoori, Thakkar, et al., 2017; H. Y. Chen et al., 1999; Häggström et al., 2012; Jawad et al., 2017; Meng et al., 2017). As well-established in the literature, CO_2 can stabilize the catalyst by eliminating coke through the reverse Boudouard reaction ($CO_2 + C \leftrightarrow 2CO$; $\Delta H_{298\,K} = +172$ kJ mol^{-1}) (Atanga et al., 2018; da Silva et al., 2015; Osaki, 2015). Among the investigated materials, zeolite-supported metal oxides that act as bifunctional catalysts offer promising performance in CO_2 capture and utilization

through cooperative interactions between BrØnsted/ Lewis acid sites on zeolite and active metal centers which lead to improved stability and selectivity (Atanga et al., 2018).

The effects of CO_2 co-feeding on catalyst performance are not clear and researchers have yet to reach a consensus on the exact role of CO_2 in various utilization reactions. For instance, De Lima and co-workers added CO_2 as a co-feed to the ethanol steam reforming process and reported enhanced stability of Pt/CeO2 catalyst and high selectivity towards hydrogen (de Lima et al., 2010). In another investigation, Díaz and co-workers studied the influence of CO_2 co-feeding on Fischer-Tropsch fuels production over carbon nanofibers supported cobalt catalyst and found that the presence of CO_2 favors the formation of lighter hydrocarbons (Fields & Backofen, 1957). Xu and co-workers developed metal modified ZSM-5 catalysts for the methanol to aromatics conversion (MTA) under the CO_2 flow. It was demonstrated that the catalysts doped with Zn, Ni, and Ag were capable of increasing the total aromatics yield in the CO_2 atmosphere (C. Xu et al., 2017).

Among heterogeneous catalysts studied for the methanol to hydrocarbons (MTH) reaction, HZSM-5 and SAPO-34 materials with a number of metal promoters such as Ga_2O_3, Cr_2O_3, CuO, ZnO, MoO_3, and Y_2O_3 are found to be the most efficient catalysts owing to their unique pore network, high chemical and thermal stability as well as bifunctional properties (Barbosa et al., 2008; Freeman et al., 2001; Hwang & Bhan, 2017; Mentzel et al., 2009; Rownaghi & Hedlund, 2011; Yan et al., 2008). Literature shows that the catalytic behavior of HZSM-5 and SAPO-34 materials for chemical transformation reactions is highly dependent on catalyst synthesis conditions, zeolite framework, and metal promoters (Xin Li et al., 2016a).

For practical applications, the synthesized powder materials need to be formed into monoliths or pellets before utilization at chemical industry (Rezaei & Webley, 2009). Zeolite monoliths are structured materials with parallel gas flow channels (Rezaei & Webley, 2012). The shape, channel size, and textural (i.e. pore distribution and exposed surface), and structural properties (e.g. active phase and amorphization) could be fine-tuned and precisely controlled in monolithic catalysts. Previous studies have examined structure property relationships of ZSM-5 monolith and their powder counterpart (Xin Li, Alwakwak, Rezaei, & Rownaghi, 2018; Xiping Li, Liu, Gong, Yang, et al., 2018a). Ivanova et al. (Ivanova et al., 2007) reported higher activity and selectivity for ZSM-5@β-SiC monolith than those for catalyst powder prepared under the same synthesis conditions. Tao et al. (Tao et al., 2003) prepared a highly crystalline meso-ZSM-5 monolith that consisted of both micropores and mesopores by using a template of carbon aerogel to impart uniform mesoporosity to the zeolite. Beers et al. (Beers et al., 2001) coated H-BEA, H-FAU on a cordierite ($2Al_2O_3 \cdot 5SiO_2 \cdot 2MgO$) monolithic substrate, and the coated monoliths resulted in an active and selective integrated catalyst-reactor configuration for the acylation of aromatics.

Recently, additive manufacturing by 3D printing has gained worldwide attention in the formulation of porous materials into practical contactors as a result of flexibility in design alteration and preparation of robust and complex geometries which requires fewer steps and minimal resources in comparison to the previously established extrusion process (Freiding & Kraushaar-Czarnetzki, 2011; Mitchell et al., 2012; Williams, 2001). Most recently, a number of porous materials such as zeolites (ZSM-5, Y, SAPO-34), metal-organic frameworks (MOFs) and Cu/Al2O3 monoliths have been fabricated by 3D printing

and used for catalysis and gas separation applications (Lefevere et al., 2017, 2018a; Thakkar et al., 2018a; Thakkar, Eastman, Al-Mamoori, et al., 2017; Thakkar, Eastman, Al-Naddaf, et al., 2017). For instance, Rezaei and co-workers developed 3D-printed porous materials such as zeolite 5 A and 13X monoliths, MOFs, aminosilicates and polymer-zeolite composites and confirmed their adsorption efficacy for CO_2 capture process (Lawson et al., 2018; Thakkar et al., 2016, 2018b; Thakkar, Eastman, Al-Mamoori, et al., 2017; Thakkar, Eastman, Al-Naddaf, et al., 2017). Couck et al. (Couck et al., 2017, 2018) produced SAPO-34 zeolite-based monolith with honeycomb shape and utilized in CO_2/N_2 separation. Lefevere et al. studied the effect of binders on mechanical and acidity of 3D-printed ZSM-5 zeolite (Lefevere et al., 2017, 2018b). In our previous works (Xin Li, Alwakwak, Rezaei, & Rownaghi, 2018; Xin Li, Rezaei, & Rownaghi, 2018; Xingfeng Li & Akagi, 2019; Xiping Li, Liu, Gong, Yang, et al., 2018b), we synthesized hierarchical ZSM-5 zeolite monoliths with macro-meso-microporsity using the 3D printing technique. The 3D-printed monolithic catalysts exhibited a more stable activity in nhexane cracking and higher selectivity to light olefins than their powder counterpart (Xin Li, Alwakwak, Rezaei, & Rownaghi, 2018; Xiping Li, Liu, Gong, Yang, et al., 2018b).

In consideration of improved catalytic performance over 3D-printed zeolite monoliths, the objective of this study was to develop monolithic catalysts comprising Ga_2O_3-, Cr_2O_3-, CuO-, ZnO-, and Y_2O_3-doped ZSM-5 and demonstrate their catalytic efficacy as bifunctional catalysts in MTH reaction with CO_2 co-feeding in order to establish a useful guideline for extrapolating, normalizing, and correlating between monolith catalyst properties and performance. The activity of the catalysts and the selectivity to light

olefins and BTX (benzene, toluene, and xylene) were compared in the presence and absence of CO_2.

2. EXPERIMENTAL SECTION

2.1. PREPARATION OF THE 3D-PRINTED MONOLITH

ZSM-5 zeolite (SiO_2/Al_2O_3 mole ratio of 50) monoliths were synthesized from ammonia-ZSM-5 powder (CBV 5524 G, Zeolyst). The commercial zeolite powder was first calcined at 550 °C for 6 h to produce proton-form of ZSM-5. In the next step, approximately 87.5 wt. % calcined ZSM-5 powder was mixed with 10 wt. % bentonite clay binder (Sigma-Aldrich) using an agitator (Model IKA-R25). Sufficient deionized water was then added to the mixture until a homogeneous slurry was formed, followed by the addition of a plasticizer, methyl cellulose (Sigma-Aldrich), to generate an aqueous paste with extrudable viscosity under stir. The paste was filled into a 10 mL syringe (Techcon Systems) furnished with a 0.60mm nozzle. The synthesis of the monolith was perform on a lab-scale 3D printer and the printing paths of which was designed by AutoCAD and coded by Slic3r in advance. The paste was dispensed and deposited on an alumina substrate in a layer-by-layer manner to produce a honeycomb-like monolith. The 3D-printed monoliths were dried overnight and then calcined for 6 h at 600 °C to remove methyl cellulose. The cross sectional surface of the cylinder monolith possessed 50% infill density resulting in a 0.60mm wall thickness. For the metal doped ZSM-5 monoliths, approximately 10 wt. % of metal in its nitrate form was added to the zeolite/bentonite mixture and rolled with grinding medium overnight to obtain a homogenous slurry. Metal dopants were added into the

zeolite paste before printing, thus eliminating the additional step of ion-exchange or impregnation that are commonly used for doping zeolite catalysts. The precursors used were Cr $(NO_3)_3 \cdot 9H_2O$, Cu $(NO_3)_2 \cdot 2.5H_2O$, Ga $(NO_3)_3 \cdot xH_2O$, Y $(NO_3)3 \cdot 6H_2O$, and Zn $(NO_3)_2 \cdot 6H_2O$ (Sigma-Aldrich). The rest of preparation steps were the same as the bare ZSM-5 monolith preparation steps.

2.2. CATALYSTS CHARACTERIZATION

X-ray diffraction (XRD) analysis was performed on a PANalytical X'Pert multipurpose X-ray diffractometer in the angle (2θ) range of 5°–50° with Cu-Kα1 radiation (40 kV and 40 mA) at a rate of 2.0° min^{-1}. Nitrogen physisorption measurements were performed on a Micromeritics 3Flex surface characterization analyzer at 77 K. Prior to the measurements, the samples were degassed at 300°C in vacuum for 6 h. Total surface area was determined by the Brunauer-Emmett-Teller (BET) method using the relative pressure (P/Po) in the range of 0.05- 0.3. The total pore volume was calculated at the P/Po = 0.99 whereas the micorpore volume was estimated by t-plot methods. The bulk composition of the materials was determined using a Perkin-Elmer Emission Spectrometer Model Plasma 1000 inductively coupled plasma-atomic emission spectrometer (ICP-AES). The dispersion of doped metals of the 3D-printed monoliths was analyzed by energy dispersive X-ray spectrometry (EDX).

Temperature-programmed desorptions of ammonia and CO_2 (NH_3- TPD, CO_2-TPD) were carried out to investigate the acidic and basic properties of the metal-doped 3D-printed ZSM-5 monolith catalysts. Both NH_3 and CO_2 adsorptions were performed on the Micromeritics 3Flex analyzer under a flow of 5% NH_3/He or CO_2/He at 100 °C. The

desorptions of NH_3 or CO_2 were measured from 100 to 600 °C at a constant ramp rate of 10 °C min_{-1}. A mass spectroscopy (BELMass) was used to detect the quantity of desorbed NH_3 and CO_2. Temperatureprogrammed reduction with hydrogen (H_2-TPR) was performed from 50 to 850 °C under a flow of 5% H_2/He using the same instrument. The functional groups of the catalysts were determined by the FTIR spectra, obtained on a Nicolet-FTIR Model 750 spectrometer. Thermogravimetric analysis-differential thermal analysis (TGA-DTA) of the spent catalysts was carried out from 30 to 900 °C using TGA (Model Q500, TA Instruments), at a rate of 10 °C min^{-1} in a 60 mL min^{-1} air flow.

2.3. MTH REACTION

The catalytic performance of 3D-printed monoliths in methanol conversion reaction was evaluated in a down-flow fixed-bed reactor setup. Nitrogen flow saturated with methanol at 30 °C was fed into the stainless-steel reactor with an inner diameter of 10 mm. The feed flow rate was controlled by a mass flow controller (Brooks, 5850). In a typical run, 0.3 g of catalyst was tested under 400 °C at 1.01 bar with a weight hourly space velocity (WHSV) of 0.35 h^{-1}. The catalyst was activated in-situ at 550 °C under nitrogen flow for 2 h. The products were directly transferred to an on-line gas chromatography (SRI 8610C) and analyzed every hour with a flame ionized detector (GC-FID) connected to mxt-wax/mxt-alumina capillary column. The inlet line to the reactor was kept heated at 110 °C, whereas the effluent line of the reactor until GC injector was kept at 145 °C to prevent potential condensation of hydrocarbons. For the reaction under CO_2 atmosphere, the nitrogen was substituted with CO_2 while keeping other test conditions the same.

3. RESULTS AND DISCUSSION

3.1. CHARACTERIZATION OF THE 3D-PRINTED MONOLITHS

The XRD patterns shown in Figure 1 indicate that structure and crystallinity of ZSM-5 zeolite were retained after printing for both pure ZSM-5 and doped-ZSM-5 monoliths with various metals. The peaks observed at 2θ=8.0, 9.0, 14.8, 22.9, 24.0 and 29.8°, were related to (101), (200), (301), (501), (303), and (503) planes, respectively, which verified the typical MFI structure (Xin Li, Rezaei, Ludlow, et al., 2018). For Cr/ZSM-5, the appearance of additional peaks at 2θ=33.6°, 36.1° and 41.5° suggested the formation of Cr_2O_3 (Mimura et al., 2006). Several peaks with less intensity were also observed at 2θ=35.6° and 38.7° for Cu/ZSM-5, and at 2θ=36.2° for Zn/ ZSM-5, which indicated the formation of CuO and ZnO, respectively in these materials (C. Xu et al., 2017) (Ereña et al., 1998). On the other hand, Ga/ZSM-5 and Y/ZSM-5 showed no observable peaks for their corresponding metal oxides. This might be due to the high dispersion of the oxides in the zeolite monoliths which made them difficult to detect by XRD beam (Hwang & Bhan, 2017) (Freeman et al., 2002).

The FTIR spectra of the investigated catalysts, shown in Figure 2, provided another aspect to confirm the ZSM-5 structure of the 3Dprinted monoliths. The peak at about 450 cm^{-1} was ascribed to the vibration of internal Si-O or Al-O bonds of the SiO_4 or AlO_4 tetrahedra, whereas the peak observed at 560 cm^{-1} was associated with external bonds of double five-member ring (Jansen et al., 1984).

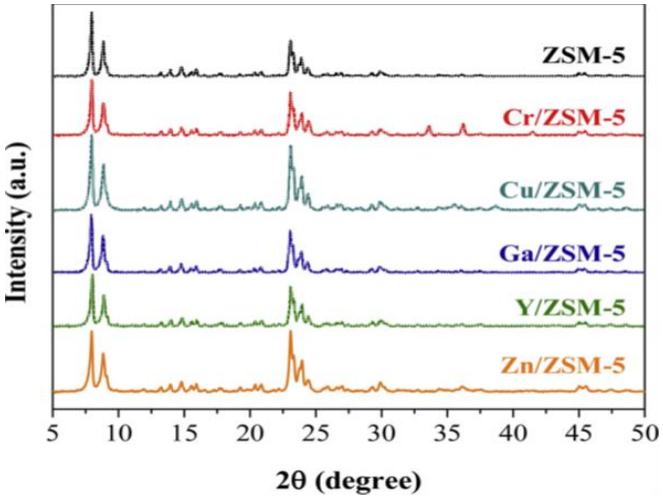

Figure 1. XRD patterns of the bare and Cr, Cu, Ga, Y, and Zn-doped 3D-printed ZSM-5 monoliths

In addition, the peak at 810 cm^{-1} was corresponded to symmetric stretching of external bonds between tetrahedral, whereas the strongest absorption peak appeared about 1110 cm^{-1} was related to the internal asymmetric stretching of Si-O-Si(Al) bonds (Barros et al., 2008). An additional band observed at around 1240 cm^{-1} was associated with the asymmetric stretching vibration of Al-O or Si-O bonds. The presence of these peaks clearly indicated that the catalysts retained their MFI structure after metal doping, in accordance with the XRD results, discussed earlier.

The Bands for hydroxyl groups (−OH) were also detected in the range of 4000-3200 cm^{-1}. The peak appeared at 3745 cm^{-1} was related to the vibration of −OH groups connected to the silicon atom (Si−OH), which were mostly on the external surface of the zeolite (Liu et al., 2015). The bands observed at 3665-3610 cm^{-1} were ascribed to the hydroxyl groups connected by Al−OH bonds. Specifically, the band at 3655 cm^{-1} was associated with the external Al-bonded hydroxyl groups with weak Brønsted acidity while the band at 3620 cm^{-1} was associated with the internal bridging hydroxyl groups (Si−OH-

Al) with strong Brønsted acidity (Olsbye et al., 2012). For Cr/ZSM-5, Cu/ZSM-5 and Zn/ZSM-5 samples, the intensity of the bands in this range remained relatively high, indicating the intact hydroxyl groups but formation of metal oxide on zeolite surface.

The textural properties of the monolith catalysts determined by N_2 physisorption measurements as well as the actual metal loading measured by elemental analysis (ICP-AES) are listed in Table 1. Due to the addition of binder and further calcination of fresh monoliths and decomposition of the plasticizer, the BET surface area of 3D-prinetd ZSM-5 monolith was reduced from 429 $cm^2\ g^{-1}$ to 373 $cm^2\ g^{-1}$, while mesopore volume increased from 0.170 $cm^3\ g^{-1}$ to 0.200 $cm^3\ g^{-1}$. Results of ICP-AES revealed that the actual metal contents were close to the nominal loading (10 wt. %) and all metal-doped monoliths contained approximately 10 wt. % metal. Furthermore, it was noticed that the metal dopants slightly decreased both the total surface area and the pore volume of the monoliths, which was close to the theoretical values added into the zeolite paste before printing. The change of the micropore volume was less significant than the change in the mesopore volume after metal incorporation, suggesting that the decrease in pore volume resulted from the metal dopant clogging in the mesopores of the monolith.

The distribution of doped metals within the ZSM-5 monolith was investigated by elemental mapping. The successful incorporation of metal particles was further confirmed by the presence of corresponding metal, oxygen, Si and Al in the EDX patterns and element mappings (Figure 3), which proved that the metal oxide nanoparticles were distributed homogeneously within the 3D-printed ZSM-5 monoliths. The acidic properties of the 3D-printed monoliths were characterized by NH_3-TPD and the results are shown in Figure 4. All samples exhibited two desorption peaks at around 102 and 413 °C, which were due to

the presence of the weak acid sites (Brønsted and/or Lewis sites) and strong Brønsted acid sites, respectively.

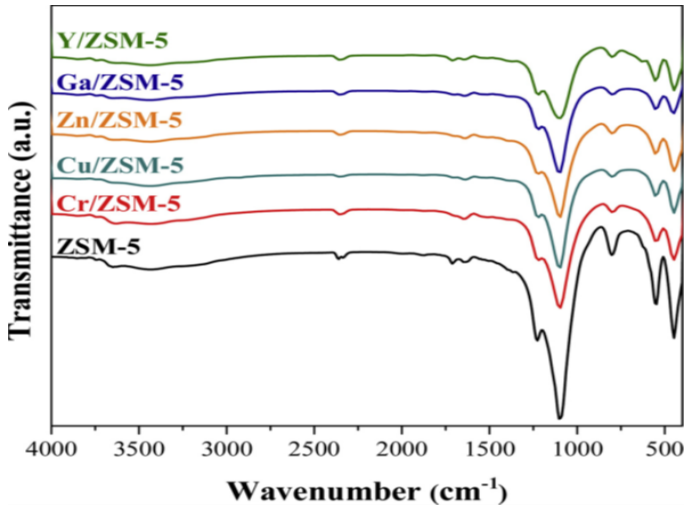

Figure 2. FITR spectra of the bare and Cr, Cu, Ga, Y, and Zn-doped 3D-printed.

Table 1. Surface area, pore volumes, and metal content of the 3D-printed ZSM-5 monoliths.

Sample	Surface area (m^2g^{-1})[a]	Total Pore volume (cm^3g^{-1})[b]	Micropore volume (cm^3g^{-1})[c]	Mesopore volume (cm^3g^{-1})[c]	Metal loading (wt.%)[d]
ZSM-5(powder)	429	0.300	0.130	0.170	-
ZSM-5(monolith)	373	0.300	0.100	0.200	-
Cr/ZSM-5	286	0.219	0.090	0.129	10.6
Cu/ZSM-5	297	0.202	0.096	0.106	9.8
Ga/ZSM-5	318	0.213	0.096	0.117	10.0
Y/ZSM-5	293	0.208	0.090	0.118	10.3
Zn/ZSM-5	285	0.227	0.090	0.137	10.3

[a] S_{BET} was obtained by analyzing nitrogen adsorption data at −196 °C in a relative vapor pressure ranging from 0.05 to 0.30.
[b] Total pore volume was estimated based on the volume adsorbed at P/P_o=0.99.
[c] Micropore area and micropore volume were determined using t-plot method.
[d] The metal loading was measured by ICP.

As summarized in Table 2, metal loading slightly increased the surface acidity (number of acid sites and/or acid strength) of the metal doped-3D-printed monoliths except for Cr/ZSM-5 monoliths. It should be noted here that the Cr/ZSM-5 monolith displayed the same profile shape as the bare ZSM-5 monolith mainly because the chromium existed in its oxide form, as confirmed by XRD analysis. These results indicated that the acidity was barely affected by the chromium dopant. Moreover, for Cr-, Ga-, Y-, and Zn-doped 3D-printed ZSM-5 monoliths, the maximum of the peaks slightly shifted to the lower temperatures. The decrease of the second desorption peak was consistent with the high exchange degree of Brönsted acid sites in these samples leading to decrease in strong acid sites. A similar reduction in desorption temperature and density of strong acid sites was observed by Veses et al. (Veses et al., 2015a) who prepared Ga-, Cu-, Sn-, and Ni-ZSM-5 catalysts.

For Cu/ZSM-5, the strength of acid sites was dramatically enhanced by the addition of copper, which is in consistent with previously reported work (Veses et al., 2015b). The ZSM-5 monoliths with Ga and Y dopants also exhibited similar TPD profiles to the bare ZSM-5 monolith, indicating that the addition of these metals to ZSM-5 had little effect on the acid strength, which might be due to the formation of micro metal oxide particles. In the case of Zn/ZSM-5, the second peak became less noticeable implying the reduced number of strong Brønsted acid sites, however, the total amount of weak acid sites, reflected by the peak area, was obviously increased, suggesting the zinc dopant converted the strong acid sites to the weak sites.

This might be the result of the exchange of the proton on the hydroxyl group by Zn^{2+}, or substitution interaction between Zn^{2+} and protons of Si−OH-Al groups to form

Zn $(OH)^+$ (Abdelsayed et al., 2015). Whereas the peaks at 377 and 657 °C for Zn/ZSM-5 can be assigned to ZnO and zinc cations, respectively.

To analyze the strength of the basic sites of Cr-, Cu-, Ga-, Y-, and Zn doped 3D-printed ZSM-5 monolith catalysts, the CO_2-TPD experiments were conducted and the profiles are shown in Figure 6. The characteristic peaks and their corresponding desorption temperature, which are indicative of amount of base sites (basicity) and base strength in the monoliths are also summarized in Table 3.

It was revealed that total basicity of monoliths decreased in the order of Zn/ZSM-5>Y/ZSM-5>Cr/ZSM-5>Cu/ZSM-5>Ga/ZSM-5>ZSM-5, which are in good agreement with adsorption of CO_2 over Lewis acidic sites of metal oxides. Basic properties of the materials depends upon the temperature profile in weak (< 200 °C), moderate (200–450 °C), and strong range (> 450 °C), respectively. As expected, no CO_2 desorption peak was observed in the spectrum of bare ZSM-5 monolith, whereas the appearance of the desorption peaks in the spectra of metal doped-ZSM-5 monoliths demonstrated the interactions between the doped metals and CO_2 molecules and that the enhancement of the basicity of the doped samples.

As Figure 6 shows, all metal-doped ZSM-5 monoliths displayed first desorption peak in the range of 100–200 °C, which implied that they contained predominantly week basic sites. In particular, Y/ZSM-5 and Ga/ZSM-5 monoliths exhibited high-intense peaks in this temperature range, indicating that the loading of Y and Ga only increased the number of weak adsorption active sites and did not enhance the overall adsorption strength. The weak adsorption of CO_2 over Y/ZSM-5 and Ga/ZSM-5 monoliths limits its contact with the catalyst sites and thus weakens the consumption of hydrogen, which could increase the

aromatics yield. The CO_2 desorption peaks for Cr-, Cu-, and Zn-doped ZSM- 5 monoliths were shifted to higher temperature, indicating strong interaction of the catalytic active sites with CO_2. The higher amount of moderate and strong active sites can activate the adsorbed CO_2 to react with hydrogen in the reactor, thus enhance the yield of the aromatic hydrocarbons consequently (C. Xu et al., 2017).

Figure 3. EDX analysis and corresponding mapping of the elements in Cr/ZSM-5, Cu/ZSM-5, Ga/ZSM-5, Y/ZSM-5, and Zn/ZSM-5 monoliths.

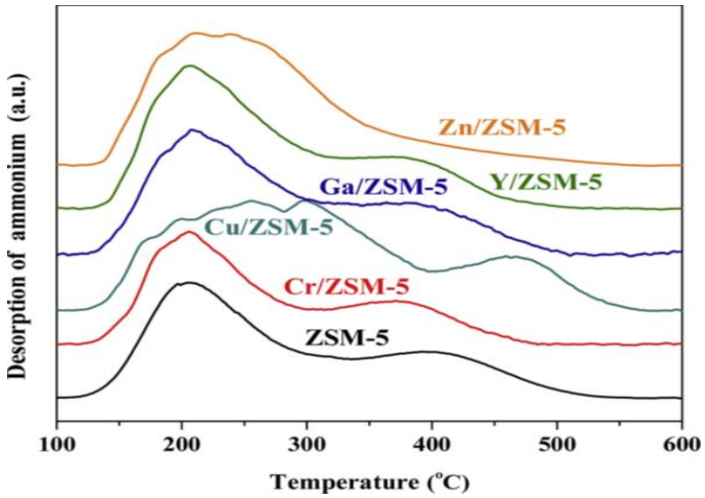

Figure 4. NH_3-TPD profiles of the bare and Cr-, Cu-, Ga-, Y-, and Zn-doped 3Dprinted ZSM-5 monoliths.

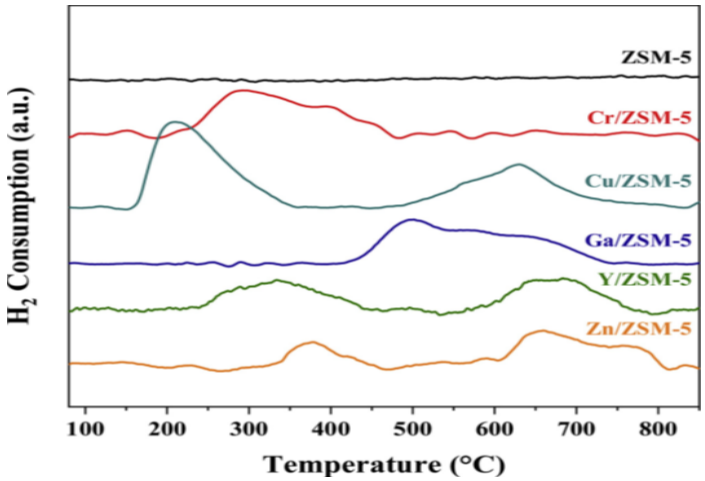

Figure 5. H_2-TPR profiles of the bare and Cr-, Cu-, Ga-, Y-, and Zn-doped 3Dprinted ZSM-5 monoliths.

3.2. MTH REACTION IN THE PRESENCE AND ABSENCE OF CO_2

Methanol conversion was carried out at 400 °C and atmospheric pressure over bare and Cr-, Cu-, Ga-, Y-, and Zn-doped 3D-printed ZSM-5 monoliths. To probe the advantages of 3D-printed ZSM-5 monolith over its powder counterpart, a control experiment was performed in which the ZSM-5 powder and the bentonite clay (binder)

with the same ratio as in the monolith were physically mixed and the reaction progress over it was monitored. As shown in Figure 7a, it was observed that the methanol conversions were of the same at the beginning of the reaction, however, the methanol conversion decreased over time from about 95 to 90% over powder catalyst due to the carbon formation and deactivation. Since the composition (ratio of the zeolite/clay) in these two forms was the same, the better performance of the monolith catalyst could be thus correlated to its 3D-printed monolith structure.

Figure 7 illustrates CH_3OH conversion in the presence and absence of CO_2 as a function of time-on-stream over the investigated monolith catalysts as well as the CO_2 conversion in the CO_2 atmosphere. It is evident that all monolith catalysts exhibited higher methanol conversion in the absence of CO_2 (under N_2 atmosphere). The trend for CO_2 conversion was more stable than methanol conversion over all the monolith under the same condition. The conversion CO_2 was less than 10% over the bare ZSM-5 (both powder and

Table 2. Summary of NH_3-TPD and H_2-TPR results.

Sample	H_2 reduction peak[a]		TPR peak area[a] (a.u.) × 10^{-8}	Weak acid peak[b]		Strong acid peak[b]		Total
	No.	T (°C)		T (°C)	Amount (mmol g^{-1})	T (°C)	Amount (mmol g^{-1})	Amountb (mmol g^{-1})
ZSM-5	-	-	-	210	0.4	394	0.16	0.56
Cr/ZSM-5	a	285	4.55	205	0.33	372	0.11	0.44
Cu/ZSM-5	a	206	5.67	279	0.56	459	0.15	0.72
	b	625	4.25					
Ga/ZSM-5	a	501	8.33	207	0.46	364	0.12	0.58
Y/ZSM-5	a	331	2.72	208	0.52	385	0.07	0.59
	b	686	2.68					
Zn/ZSM-5	a	376	0.96	208	0.54	375	0.06	0.6
	b	567	2.53					
	c	761	0.76					

[a] Obtained from H_2-TPR results.
[b] Obtained from NH_3-TPD results

Table 3. Summary of CO_2-TPD results.

Peak #	Sample	ZSM-5	Cr/ZSM-5	Cu/ZSM-5	Ga/ZSM-5	Y/ZSM-5	Zn/ZSM-5
1	T (°C)	-	114	107	114	131	101
	Peak area (mmol/g)	-	0.012	0.027	0.099	0.425	0.006
2	T (°C)	-	289	413	484	401	165
	Peak area (mmol/g)	-	0.055	0.194	0.099	0.142	0.004
3	T (°C)	-	402	615	683	759	217
	Peak area (mmol/g)	-	0.128	0.029	0.042	0.337	0.014
4	T (°C)	-	486	754	-	-	481
	Peak area (mmol/g)	-	0.203	0.013	-	-	0.060
5	T (°C)	-	653	-	-	-	363
	Peak area (mmol/g)	-	0.053	-	-	-	0.072
6	T (°C)	-	-	-	-	-	450
	Peak area (mmol/g)	-	-	-	-	-	0.137
7	T (°C)	-	-	-	-	-	742
	Peak area (mmol/g)	-	-	-	-	-	0.271

monolith) and Ga/ZSM-5 monoliths and remained constant over the time-on-stream. Among all the 3D-printed monoliths, Y/ZSM-5 monolith resulted the lowest CO_2 conversion due to high density of weakly basic sites providing for low interaction of yttrium oxide with CO_2. As for the Y/ZSM-5 monolith, the conversion of both methanol and CO_2 in the presence of CO_2 was more stable than those over other monoliths.

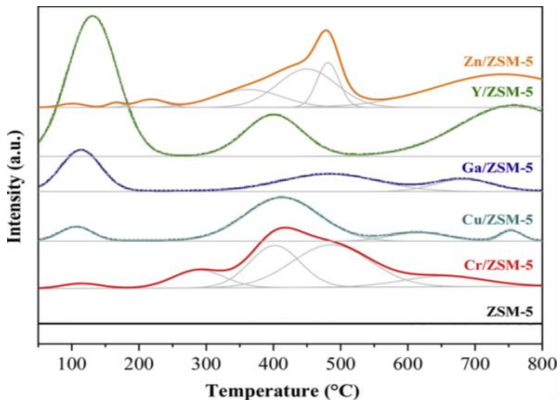

Figure 6. CO_2-TPD profiles of the bare and Cr-, Cu-, Ga-, Y-, and Zn-doped 3Dprinted ZSM-5 monoliths.

The methanol conversions were about 95 and 75% within 360 min in the absence and presence of CO_2, respectively According to the H_2-TPR profiles, yttrium oxide was present in both metal and cation forms, which exchanged the H+ in the zeolite framework, as the latter peak indicated. From Table 2, there were less strong acid sites and more weak acid sites on Y/ZSM-5 than on the bare ZSM-5. Therefore, a combination of high density of weakly basic sites of the doped metals and ZSM-5 catalytic function itself selectively decomposes methanol and enhances the formation of light olefins. As evident from N_2 physisorption results, the altered porosity might also be a factor that affects the activity.

Notably, the Cr/ZSM-5 monolith exhibited the highest selectivity to propylene with the highest CO_2 conversion (20–40%). Previous research has shown that in the presence of CO_2, Cr^{3+} and Cr^{2+} sites participate additionally in an alternative oxidative pathway for propylene formation (Atanga et al., 2018). The methanol conversion over Cu/ZSM-5 monolith experienced a sharp decrease at 120 min followed by an increasing trend within 360 min from 50 to 78%. The maximum methanol conversion was achieved for Y/ZSM-5 in the presence and absence of CO_2 within this series of monolith catalysts. Moreover, bare and metaldoped 3D printed ZSM-5 monoliths show more than 90% methanol conversion due to the relatively same density of acid sites. Linking both methanol and CO_2 conversion with the NH_3-TPD and CO_2-TPD profiles, it can be concluded that high population of moderate surface base sites in Cr/ZSM-5, Cu/ZSM-5, and Zn/ZSM-5 monoliths were responsible for catalyst stability in the presence of CO_2.

As the major hydrocarbon products in methanol conversion processes, especially emphasized in MTH reaction, light olefins (i.e. ethylene, propylene, and butylene) are always considered. Figure 8 shows the selectivity towards light olefins over 3D-printed

monoliths under two different atmospheres. As shown in Figure 8 and Table 4, the light olefins selectivity has been reduced over all 3D-printed ZSM-5 monoliths in the presence of CO_2, nevertheless, the catalyst stability improved due to reverse Boudouard reaction, which prevents deposition of active carbon species on the metal surface. Moreover, this could be due to the difference in the particle size, reducibility of metals and surface texture of the metal oxides. From the detailed hydrocarbon product distribution data shown in Table 4, it can be noted that the reduction in the light olefins are mainly ethylene. Generally, the acidity increases the number of sites responsible for adsorption and polymerization of olefins (Zhu et al., 2011). These results indicate that the CO_2 co feeding promotes cracking and dehydrocyclization, leading to production of light alkanes (methane and ethane) and BTX compounds.

Figure 9 shows the effect of CO_2 co-feeding on BTX selectivity over 3Dprinted monoliths in MTH reaction. The product distribution for methanol conversion over bare and metal doped-ZSM-5 monolith catalysts in the presence and absence of CO_2 are summarized in Table 4. As evident from these results, the effect of CO_2 on BTX selectivity varied with the type of doped metal. For instance, although the selectivity towards BTX were significantly reduced over Cr/ZSM-5, Cu/ZSM-5, and Ga/ZSM-5 monolith catalysts in the presence of CO_2, CO_2 co-feeding favored the formation of BTX over Y/ZSM-5 and Zn/ZSM-5 monoliths. The BTX selectivity over Y/ZSM-5 and Zn/ZSM-5 reached 26 and 29%, respectively. It indicated that the ZSM-5 catalysts modified with these two metals can catalyze the reaction of CO_2 with H_2, which was generated in the methanol conversion, thereby consuming hydrogen atoms and reducing the formation of alkanes, as shown in Table 4, thus improving the yield of BTX [15]. The catalytic results also suggested that

higher weak surface acidity and lower strong surface acidity favored ethylene and propylene production, whereas presence of CO_2 led to the production of more ethane. Thus, the weak to moderate surface acid density are optimum for the selective conversion of methanol to propylene in the presence of CO_2.

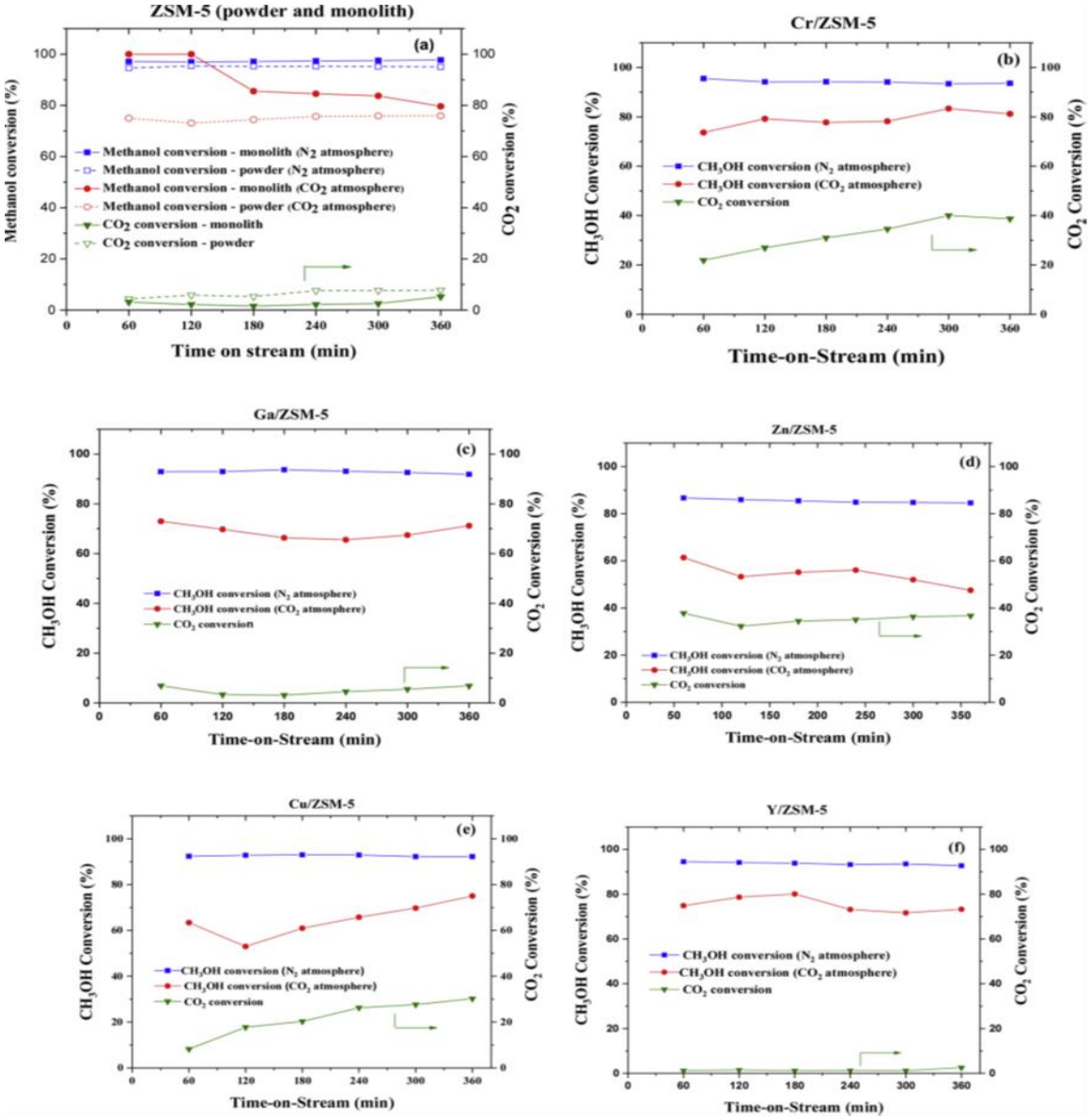

Figure 7. Methanol conversion under N_2 and CO_2 atmospheres and CO_2 conversion in the presence and absence of CO_2 as a function of time-on-stream. Reaction Temperature = 400 °C, WHSV= 0.35 h^{-1}.

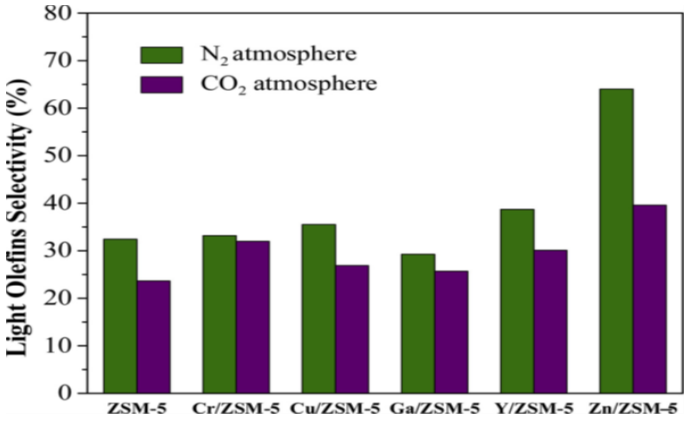

Figure 8. Light olefins selectivity over the 3D-printed monoliths with various dopants in the presence and absence of CO_2. Reaction temperature=400 °C, WHSV=0.35 h^{-1}, product samples were tested for 120 min.

Table 4. Product distribution of methanol conversion over the 3D-printed monoliths (reaction temperature = 400 °C; WHSV= 0.35 h^{-1}, product samples were tested for 120 min).

	ZSM-5		Cr/ZSM-5		Cu/ZSM-5		GaZSM-5		Y/ZSM-5		Zn/ZSM-5	
atmosphere	N_2	CO_2	N_2	CO_2	N_2	CO_2	N_2	CO_2	N_2	CO_2	N_2	CO_2
Methane	1	4.1	1	11	2	15	2.6	8.8	2	6.2	6	5.5
Ethane	0	8.1	0	9	0	14	0.9	8.5	0	10	1	12
Ethylene	12	1	12	3.5	12	2.9	11	2.2	13	3.8	25	6
Propane	9	7	6	8.8	6	7.1	7.6	7.1	8	7.1	2	1.3
Propylene	14	10	17	20	14	16	12	10	16	12	28	25
Butane	17	9.7	15	15	13	11	15	11	14	7.4	2	3.8
Butylene	7	5.2	4	7.2	9	7.8	6.3	6.1	9	7.7	11	12
Benzene	2	3.8	8	1.5	8	2.9	8.3	4.3	8	4.1	3	4
Toluene	9	15	4	0.7	3	0.9	2.5	16	2	13	4	3.3
Xylene	5	15	3	4	8	2.7	8.5	3.5	5	8.4	8	11
others	25	21	28	20	24	19	25	22	23	20	10	16

Furthermore, the effect of metal doping on BTX selectivity was not significant in the absence of CO_2, however, the ratio for benzene, toluene, and xylene dependent on the metal dopants. The BTX selectivities over Cu/ZSM-5 and Ga/ZSM-5 were slightly higher than the bare ZSM-5 monolith in the presence and absence of CO_2 which could be due to

the dehydrogenation ability of these two metals that promoted the aromatization reaction (Suganda et al., 2013; Wei et al., 2015).

The effect of surface acidity on the performance of zeolites in the MTH reaction has been investigated by several research groups (Bjørgen et al., 2004; Kim et al., 2010; Rownaghi et al., 2012). The incorporation of metal into the ZSM-5 paste enhanced the surface basicity while decreased the surface area of zeolite catalysts due to pore blockages by metal precursors. The obtained catalytic results demonstrated that metal doping enhances the catalyst stability in the absence of CO_2 due to decrease in the strong acid sites, which led to the suppression of the side reactions such as oligomerization and aromatization. Moreover, as shown in Table 3 and Figure 7, with increasing the surface basicity, the activity of catalyst was enhanced in the presence of CO_2.

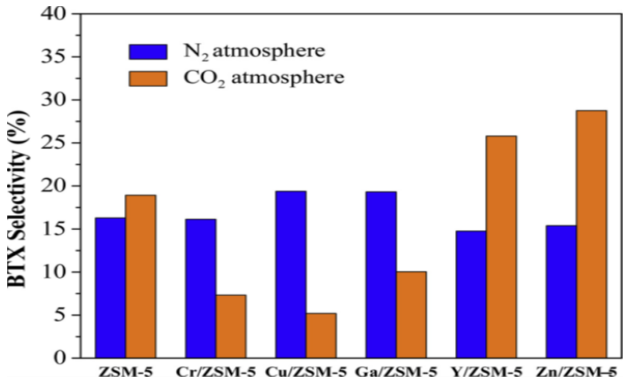

Figure 9. BTX selectivity over the 3D-printed monoliths with various dopants in the presence and absence of CO_2. Reaction temperature, 400 °C, WHSV=0.35 h^{-1}, product samples were tested for 120 min.

Figure 10. Shows the amount of carbonaceous deposits on the bare and Cr-, Cu-, Ga-, Y-, and Zn-doped 3D-printed ZSM-5 monoliths after methanol conversion at 400 °C for 6 h time-on-stream in N_2 and CO_2 atmospheres. In general, the amount of carbonaceous

products deposited in the presence of CO_2 was significantly lower than that in N_2 atmosphere over the same monoliths. All samples experienced a weight loss at around 100 °C, which was assigned to the moisture in the samples. Among all 3D-printed ZSM-5 monoliths, the amount of carbonaceous deposition was highest on Y/ZSM-5 and lowest over Cu/ZSM-5. Compared with the bare 3D-printed ZSM-5 monolith, although metal-doped 3D-printed ZSM-5 monoliths exhibited high selectivity toward light olefins and BTX compounds, they were rapidly deactivated due to coke deposition, which completely blocked the internal channels of the monoliths in the absence of CO_2. On the contrary, the amount of coke deposited on all metal-doped 3D-printed ZSM-5 monoliths (except Zn/ ZSM-5) was lower than on the bare ZSM-5 in the presence of CO_2 mainly due to reverse Boudouard reaction which can improve the catalyst stability. As shown in Table 2, Zn-doped 3D-printed ZSM-5 monolith gave rise to higher amount of propylene in the presence of CO_2, which is the precursor for further carbon deposition.

4. CONCLUSION

Herein, we reported the preparation ZSM-5 zeolite monoliths with various metal dopants using 3D printing technique. The metal dopants were added directly to the zeolite paste before printing. The catalytic behavior of these novel materials was evaluated in methanol conversion reaction under N_2 and CO_2 atmosphere. Characterization results of the catalysts suggested that the physiochemical properties of the ZSM-5 were modified by incorporation of metal dopants. The catalytic results indicated that the product distribution varied with the type of metal doped, and that methanol conversion was

influenced by the acidity and basicity of the monoliths catalyst in the presence of CO_2. Combined CO_2-TPD, NH3-TPD, and catalytic evaluation results demonstrated that the metal-doped ZSM-5 monolith possessed more weak to moderate acid and basic sites,

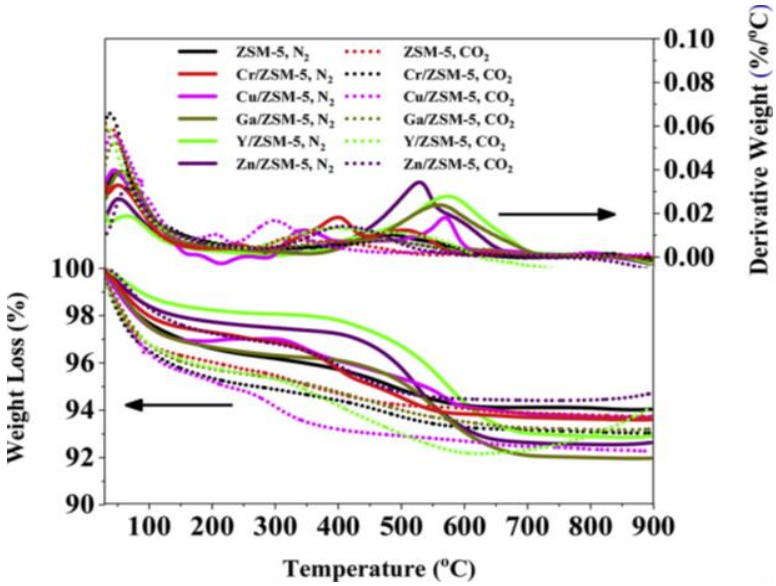

Figure 10. TGA (lower) and DTA (upper) profiles of the spent catalysts after 6 h of methanol conversion at 400 °C in the presence and absence of CO_2.

which accounted for its superior catalytic performance. Unlike the lower ethylene yield, the amount of propylene and BTX compounds were enhanced in the presence of CO_2 over all metal doped monoliths.

FUNDING

The authors declare no competing financial interest.

ACKNOWLEDGMENTS

We thank the University of Missouri Research Board (UMRB) and Materials Research Center (MRC) of Missouri S&T for financially supporting this work**.**

REFERENCES

Abdelsayed, V., Shekhawat, D., & Smith, M. W. (2015). Effect of Fe and Zn promoters on Mo/HZSM-5 catalyst for methane dehydroaromatization. Fuel, 139, 401–410. https://doi.org/https://doi.org/10.1016/j.fuel.2014.08.064

Al-Mamoori, A., Krishnamurthy, A., Rownaghi, A. A., & Rezaei, F. (2017). Carbon Capture and Utilization Update. Energy Technology, 5(6), 834–849. https://doi.org/10.1002/ente.201600747

Al-Mamoori, A., Thakkar, H., Li, X., Rownaghi, A. A., & Rezaei, F. (2017). Development of Potassium- and Sodium-Promoted CaO Adsorbents for CO_2 Capture at High Temperatures. Industrial and Engineering Chemistry Research, 56(29), 8292–8300. https://doi.org/10.1021/acs.iecr.7b01587

Atanga, M. A., Rezaei, F., Jawad, A., Fitch, M., & Rownaghi, A. A. (2018). Oxidative dehydrogenation of propane to propylene with carbon dioxide. Applied Catalysis B: Environmental, 220(August 2017), 429–445. https://doi.org/10.1016/j.apcatb.2017.08.052

Barbosa, F. S. R., Ruiz, V. S. O., Monteiro, J. L. F., De Avillez, R. R., Borges, L. E. P., & Appel, L. G. (2008). The deactivation modes of $Cu/ZnO/Al_2O_3$ and HZSM-5 physical mixture in the one-step DME synthesis. Catalysis Letters, 126(1–2), 173–178. https://doi.org/10.1007/s10562-008-9601-7

Barros, I. C. L., Braga, V. S., Pinto, D. S., de Macedo, J. L., Filho, G. N. R., Dias, J. A., & Dias, S. C. L. (2008). Effects of niobium addition on ZSM-5 studied by thermal and spectroscopy methods. Microporous and Mesoporous Materials, 109(1), 485–493. https://doi.org/https://doi.org/10.1016/j.micromeso.2007.05.050

Beers, A. E. W., Nijhuis, T. A., Kapteijn, F., & Moulijn, J. A. (2001). Zeolite coated structures for the acylation of aromatics. Microporous and Mesoporous Materials, 48(1), 279–284. https://doi.org/https://doi.org/10.1016/S1387-1811 (01)00368-7

Bjørgen, M., Olsbye, U., Petersen, D., & Kolboe, S. (2004). The methanol-to-hydrocarbons reaction: insight into the reaction mechanism from [12C] benzene and [13C] methanol coreactions over zeolite H-beta. Journal of Catalysis, 221(1), 1–10. https://doi.org/https://doi.org/10.1016/S0021-9517 (03)00284-7

Chen, H. Y., Lau, S. P., Chen, L., Lin, J., Huan, C. H. A., Tan, K. L., & Pan, J. S. (1999). Synergism between Cu and Zn sites in Cu/Zn catalysts for methanol synthesis. Applied Surface Science, 152(3), 193–199. https://doi.org/https://doi.org/10.1016/S0169-4332 (99)00317-7

Chen, Z., Li, X., Xu, Y., Dong, Y., Lai, W., Fang, W., & Yi, X. (2018). Fabrication of nano-sized SAPO-11 crystals with enhanced dehydration of methanol to dimethyl ether. Catalysis Communications, 103, 1–4. https://doi.org/https://doi.org/10.1016/j.catcom.2017.09.002

Couck, S., Cousin-Saint-Remi, J., Van der Perre, S., Baron, G. V, Minas, C., Ruch, P., & Denayer, J. F. M. (2018). 3D-printed SAPO-34 monoliths for gas separation. Microporous and Mesoporous Materials, 255, 185–191. https://doi.org/https://doi.org/10.1016/j.micromeso.2017.07.014

Couck, S., Lefevere, J., Mullens, S., Protasova, L., Meynen, V., Desmet, G., Baron, G. V, & Denayer, J. F. M. (2017). CO2, CH4 and N2 separation with a 3DFD-printed ZSM-5 monolith. Chemical Engineering Journal, 308, 719–726. https://doi.org/https://doi.org/10.1016/j.cej.2016.09.046

da Silva, T. C., Pinto, J. F., Santos, F. M., dos Santos, L. T., Aranda, D. A. G., Ribeiro, F., Batalha, N., & Pereira, M. M. (2015). Vanadium and alumina modified with groups I and II elements for CO_2 and coke reaction under fluid catalytic cracking process. Applied Catalysis B: Environmental, 164, 225–233. https://doi.org/https://doi.org/10.1016/j.apcatb.2014.09.028

Dai, W., Wang, X., Wu, G., Guan, N., Hunger, M., & Li, L. (2011). Methanol-to-olefin conversion on silicoaluminophosphate catalysts: Effect of brønsted acid sites and framework structures. ACS Catalysis, 1(4), 292–299. https://doi.org/10.1021/cs200016u

de Lima, S. M., da Silva, A. M., Jacobs, G., Davis, B. H., Mattos, L. V, & Noronha, F. B. (2010). New approaches to improving catalyst stability over Pt/ceria during ethanol steam reforming: Sn addition and CO_2 co-feeding. Applied Catalysis B: Environmental, 96(3), 387–398. https://doi.org/https://doi.org/10.1016/j.apcatb.2010.02.036

Ereña, J., Arandes, J. M., Bilbao, J., Aguayo, A. T., & De Lasa, H. I. (1998). Study of Physical Mixtures of Cr2O3-ZnO and ZSM-5 Catalysts for the Transformation of Syngas into Liquid Hydrocarbons. Industrial and Engineering Chemistry Research, 37(4), 1211–1219. https://doi.org/10.1021/ie970568p

Fechete, I., Wang, Y., & Védrine, J. C. (2012). The past, present and future of heterogeneous catalysis. Catalysis Today, 189(1), 2–27. https://doi.org/https://doi.org/10.1016/j.cattod.2012.04.003

Fields, D. S., & Backofen, W. A. (1957). Terms and conditions Privacy Policy Copyright ©2017 Elsevier B.V. All rights reserved. Scopus® is a registered trademark of Elsevier B.V. Proc ASTM, 57(1970), 1259–1272.

Freeman, D., Wells, R. P. K., & Hutchings, G. J. (2001). Methanol to hydrocarbons: Enhanced aromatic formation using a composite Ga_2O_3-H-ZSM-5 catalyst. Chemical Communications, 1(18), 1754–1755. https://doi.org/10.1039/b104844a

Freeman, D., Wells, R. P. K., & Hutchings, G. J. (2002). Conversion of methanol to hydrocarbons over Ga_2O_3/H-ZSM-5 and Ga2O3/WO3 catalysts. Journal of Catalysis, 205(2), 358–365. https://doi.org/10.1006/jcat.2001.3446

Freiding, J., & Kraushaar-Czarnetzki, B. (2011). Novel extruded fixed-bed MTO catalysts with high olefin selectivity and high resistance against coke deactivation. Applied Catalysis A: General, 391(1), 254–260. https://doi.org/https://doi.org/10.1016/j.apcata.2010.05.035

Furumoto, Y., Harada, Y., Tsunoji, N., Takahashi, A., Fujitani, T., Ide, Y., Sadakane, M., & Sano, T. (2011). Effect of acidity of ZSM-5 zeolite on conversion of ethanol to propylene. Applied Catalysis A: General, 399(1), 262–267. https://doi.org/https://doi.org/10.1016/j.apcata.2011.04.009

Häggström, C., Öhrman, O., Rownaghi, A. A., Hedlund, J., & Gebart, R. (2012). Catalytic methanol synthesis via black liquor gasification. Fuel Processing Technology, 94(1), 10–15. https://doi.org/10.1016/j.fuproc.2011.09.019

He, L.-N., Rogers, R. D., Su, D., Tundo, P., & Conrad Zhang, Z. (2016). Green Chemistry and Sustainable Technology Series editors. http://www.springer.com/series/11661

Hirota, Y., Murata, K., Miyamoto, M., Egashira, Y., & Nishiyama, N. (2010). Light olefins synthesis from methanol and dimethylether over SAPO-34 nanocrystals. Catalysis Letters, 140(1–2), 22–26. https://doi.org/10.1007/s10562-010-0421-1

Hwang, A., & Bhan, A. (2017). Bifunctional Strategy Coupling Y_2O_3-Catalyzed Alkanal Decomposition with Methanol-to-Olefins Catalysis for Enhanced Lifetime. ACS Catalysis, 7(7), 4417–4422. https://doi.org/10.1021/acscatal.7b00894

Ivanova, S., Louis, B., Madani, B., Tessonnier, J. P., Ledoux, M. J., & Pham-Huu, C. (2007). ZSM-5 coatings on β-SiC monoliths: Possible new structured catalyst for the methanol-to-olefins process. Journal of Physical Chemistry C, 111(11), 4368–4374. https://doi.org/10.1021/jp067535k

Jang, H.-G., Min, H.-K., Lee, J. K., Hong, S. B., & Seo, G. (2012). SAPO-34 and ZSM-5 nanocrystals' size effects on their catalysis of methanol-to-olefin reactions. Applied Catalysis A: General, 437–438, 120–130. https://doi.org/https://doi.org/10.1016/j.apcata.2012.06.023

Jansen, J. C., van der Gaag, F. J., & van Bekkum, H. (1984). Identification of ZSM-type and other 5-ring containing zeolites by i.r. spectroscopy. Zeolites, 4(4), 369–372. https://doi.org/https://doi.org/10.1016/0144-2449 (84)90013-7

Jawad, A., Rezaei, F., & Rownaghi, A. A. (2017). Porous polymeric hollow fibers as bifunctional catalysts for CO_2 conversion to cyclic carbonates. Journal of CO_2 Utilization, 21, 589–596. https://doi.org/https://doi.org/10.1016/j.jcou.2017.09.007

Kim, J., Choi, M., & Ryoo, R. (2010). Effect of mesoporosity against the deactivation of MFI zeolite catalyst during the methanol-to-hydrocarbon conversion process. Journal of Catalysis, 269(1), 219–228. https://doi.org/https://doi.org/10.1016/j.jcat.2009.11.009

Lawson, S., Al-Naddaf, Q., Krishnamurthy, A., Amour, M. S., Griffin, C., Rownaghi, A. A., Knox, J. C., & Rezaei, F. (2018). UTSA-16 Growth within 3D-Printed Co-Kaolin Monoliths with High Selectivity for CO_2/CH_4, CO_2/N_2, and CO_2/H_2 Separation. ACS Applied Materials and Interfaces, 10(22), 19076–19086. https://doi.org/10.1021/acsami.8b05192

Lefevere, J., Mullens, S., & Meynen, V. (2018a). The impact of formulation and 3D-printing on the catalytic properties of ZSM-5 zeolite. Chemical Engineering Journal, 349, 260–268. https://doi.org/https://doi.org/10.1016/j.cej.2018.05.058

Lefevere, J., Mullens, S., & Meynen, V. (2018b). The impact of formulation and 3D-printing on the catalytic properties of ZSM-5 zeolite. Chemical Engineering Journal, 349, 260–268. https://doi.org/https://doi.org/10.1016/j.cej.2018.05.058

Lefevere, J., Protasova, L., Mullens, S., & Meynen, V. (2017). 3D-printing of hierarchical porous ZSM-5: The importance of the binder system. Materials and Design, 134, 331–341. https://doi.org/10.1016/j.matdes.2017.08.044

Li, Xin, Alwakwak, A. A., Rezaei, F., & Rownaghi, A. A. (2018). Synthesis of Cr, Cu, Ni, and Y-Doped 3D-Printed ZSM-5 Monoliths and Their Catalytic Performance for n-Hexane Cracking. ACS Applied Energy Materials, 1(6), 2740–2748. https://doi.org/10.1021/acsaem.8b00412

Li, Xin, Kant, A., He, Y., Thakkar, H. V, Atanga, M. A., Rezaei, F., Ludlow, D. K., & Rownaghi, A. A. (2016a). Light olefins from renewable resources: Selective catalytic dehydration of bioethanol to propylene over zeolite and transition metal oxide catalysts. Catalysis Today, 276, 62–77. https://doi.org/https://doi.org/10.1016/j.cattod.2016.01.038

Li, Xin, Kant, A., He, Y., Thakkar, H. V, Atanga, M. A., Rezaei, F., Ludlow, D. K., & Rownaghi, A. A. (2016b). Light olefins from renewable resources: Selective catalytic dehydration of bioethanol to propylene over zeolite and transition metal oxide catalysts. Catalysis Today, 276, 62–77. https://doi.org/https://doi.org/10.1016/j.cattod.2016.01.038

Li, Xin, Rezaei, F., Ludlow, D. K., & Rownaghi, A. A. (2018). Synthesis of SAPO-34@ZSM-5 and SAPO-34@Silicalite-1 Core-Shell Zeolite Composites for Ethanol Dehydration. Industrial and Engineering Chemistry Research, 57(5), 1446–1453. https://doi.org/10.1021/acs.iecr.7b05075

Li, Xin, Rezaei, F., & Rownaghi, A. A. (2018). 3D-printed zeolite monoliths with hierarchical porosity for selective methanol to light olefin reaction. Reaction Chemistry and Engineering, 3(5), 733–746. https://doi.org/10.1039/c8re00095f

Li, Xingfeng, & Akagi, M. (2019). Improving multilingual speech emotion recognition by combining acoustic features in a three-layer model. Speech Communication, 110, 1–12. https://doi.org/https://doi.org/10.1016/j.specom.2019.04.004

Li, Xiping, Liu, F., Gong, N., Yang, C., & Wang, B. (2018a). Surface topography induced high injection joining strength of polymer-metal composite and fracture mechanism. Composite Structures, 184, 545–553. https://doi.org/https://doi.org/10.1016/j.compstruct.2017.10.020

Li, Xiping, Liu, F., Gong, N., Yang, C., & Wang, B. (2018b). Surface topography induced high injection joining strength of polymer-metal composite and fracture mechanism. Composite Structures, 184, 545–553. https://doi.org/https://doi.org/10.1016/j.compstruct.2017.10.020

Liu, B., France, L., Wu, C., Jiang, Z., Kuznetsov, V. L., Al-Megren, H. A., Al-Kinany, M., Aldrees, S. A., Xiao, T., & Edwards, P. P. (2015). Methanol-to-hydrocarbons conversion over MoO3/H-ZSM-5 catalysts prepared via lower temperature calcination: a route to tailor the distribution and evolution of promoter Mo species, and their corresponding catalytic properties. Chemical Science, 6(9), 5152–5163. https://doi.org/10.1039/c5sc01825k

Meng, X., He, H., Nie, Y., Zhang, X., Zhang, S., & Wang, J. (2017). Temperature-Controlled Reaction-Separation for Conversion of CO_2 to Carbonates with Functional Ionic Liquids Catalyst. ACS Sustainable Chemistry and Engineering, 5(4), 3081–3086. https://doi.org/10.1021/acssuschemeng.6b02612

Mentzel, U. V., Rovik, A. K., & Christensen, C. H. (2009). Co-conversion of ethane and methanol into higher hydrocarbons over Ga/H-ZSM-5, Mo/H-ZSM-5 and Ga-Mo/H-ZSM-5. Catalysis Letters, 127(1–2), 44–48. https://doi.org/10.1007/s10562-008-9726-8

Mimura, N., Okamoto, M., Yamashita, H., Ted Oyama, S., & Murata, K. (2006). Oxidative dehydrogenation of ethane over Cr/ZSM-5 catalysts using CO_2 as an oxidant. Journal of Physical Chemistry B, 110(43), 21764–21770. https://doi.org/10.1021/jp061966l

Mitchell, S., Michels, N. L., Kunze, K., & Pérez-Ramírez, J. (2012). Visualization of hierarchically structured zeolite bodies from macro to nano length scales. Nature Chemistry, 4(10), 825–831. https://doi.org/10.1038/nchem.1403

Mondal, K., Sasmal, S., Badgandi, S., Chowdhury, D. R., & Nair, V. (2016). Dry reforming of methane to syngas: a potential alternative process for value added chemicals—a techno-economic perspective. Environmental Science and Pollution Research, 23(22), 22267–22273. https://doi.org/10.1007/s11356-016-6310-4

Olsbye, U., Svelle, S., Bjrgen, M., Beato, P., Janssens, T. V. W., Joensen, F., Bordiga, S., & Lillerud, K. P. (2012). Conversion of methanol to hydrocarbons: How zeolite cavity and pore size controls product selectivity. Angewandte Chemie - International Edition, 51(24), 5810–5831. https://doi.org/10.1002/anie.201103657

Osaki, T. (2015). Effect of Nickel Diameter on the Rates of Elementary Steps Involved in CO_2 Reforming of CH_4 over Ni/Al_2O_3 Catalysts. Catalysis Letters, 145(11), 1931–1940. https://doi.org/10.1007/s10562-015-1608-2

Rezaei, F., & Webley, P. (2009). Optimum structured adsorbents for gas separation processes. Chemical Engineering Science, 64(24), 5182–5191. https://doi.org/https://doi.org/10.1016/j.ces.2009.08.029

Rezaei, F., & Webley, P. A. (2012). Optimal design of engineered gas adsorbents: Pore-scale level. Chemical Engineering Science, 69(1), 270–278. https://doi.org/https://doi.org/10.1016/j.ces.2011.10.039

Rownaghi, A. A., & Hedlund, J. (2011). Methanol to gasoline-range hydrocarbons: Influence of nanocrystal size and mesoporosity on catalytic performance and product distribution of ZSM-5. Industrial and Engineering Chemistry Research, 50(21), 11872–11878. https://doi.org/10.1021/ie201549j

Rownaghi, A. A., Rezaei, F., Stante, M., & Hedlund, J. (2012). Selective dehydration of methanol to dimethyl ether on ZSM-5 nanocrystals. Applied Catalysis B: Environmental, 119–120, 56–61. https://doi.org/10.1016/j.apcatb.2012.02.017

Suganda, R., Sutrisno, E., & Wardana, I. W. (2013). 済無No Title No Title. Journal of Chemical Information and Modeling, 53(9), 1689–1699.

Sun, Q., Wang, N., Xi, D., Yang, M., & Yu, J. (2014). Organosilane surfactant-directed synthesis of hierarchical porous SAPO-34 catalysts with excellent MTO performance. Chemical Communications, 50(49), 6502–6505. https://doi.org/10.1039/c4cc02050b

Tan, J., Liu, Z., Bao, X., Liu, X., Han, X., He, C., & Zhai, R. (2002). Crystallization and Si incorporation mechanisms of SAPO-34. Microporous and Mesoporous Materials, 53(1), 97–108. https://doi.org/https://doi.org/10.1016/S1387-1811(02)00329-3

Tao, Y., Kanoh, H., & Kaneko, K. (2003). ZSM-5 monolith of uniform mesoporous channels. Journal of the American Chemical Society, 125(20), 6044–6045. https://doi.org/10.1021/ja0299405

Thakkar, H., Eastman, S., Al-Mamoori, A., Hajari, A., Rownaghi, A. A., & Rezaei, F. (2017). Formulation of Aminosilica Adsorbents into 3D-Printed Monoliths and Evaluation of Their CO_2 Capture Performance. ACS Applied Materials and Interfaces, 9(8), 7489–7498. https://doi.org/10.1021/acsami.6b16732

Thakkar, H., Eastman, S., Al-Naddaf, Q., Rownaghi, A. A., & Rezaei, F. (2017). 3D-Printed Metal-Organic Framework Monoliths for Gas Adsorption Processes. ACS Applied Materials and Interfaces, 9(41), 35908–35916. https://doi.org/10.1021/acsami.7b11626

Thakkar, H., Eastman, S., Hajari, A., Rownaghi, A. A., Knox, J. C., & Rezaei, F. (2016). 3D-Printed Zeolite Monoliths for CO_2 Removal from Enclosed Environments. ACS Applied Materials and Interfaces, 8(41), 27753–27761. https://doi.org/10.1021/acsami.6b09647

Thakkar, H., Lawson, S., Rownaghi, A. A., & Rezaei, F. (2018a). Development of 3D-printed polymer-zeolite composite monoliths for gas separation. Chemical Engineering Journal, 348, 109–116. https://doi.org/https://doi.org/10.1016/j.cej.2018.04.178

Thakkar, H., Lawson, S., Rownaghi, A. A., & Rezaei, F. (2018b). Development of 3D-printed polymer-zeolite composite monoliths for gas separation. Chemical Engineering Journal, 348, 109–116. https://doi.org/https://doi.org/10.1016/j.cej.2018.04.178

Veses, A., Puértolas, B., Callén, M. S., & García, T. (2015a). Catalytic upgrading of biomass derived pyrolysis vapors over metal-loaded ZSM-5 zeolites: Effect of different metal cations on the bio-oil final properties. Microporous and Mesoporous Materials, 209, 189–196. https://doi.org/https://doi.org/10.1016/j.micromeso.2015.01.012

Veses, A., Puértolas, B., Callén, M. S., & García, T. (2015b). Catalytic upgrading of biomass derived pyrolysis vapors over metal-loaded ZSM-5 zeolites: Effect of different metal cations on the bio-oil final properties. Microporous and Mesoporous Materials, 209, 189–196. https://doi.org/https://doi.org/10.1016/j.micromeso.2015.01.012

Wei, Z., Xia, T., Liu, M., Cao, Q., Xu, Y., Zhu, K., & Zhu, X. (2015). Alkaline modification of ZSM-5 catalysts for methanol aromatization: The effect of the alkaline concentration. Frontiers of Chemical Science and Engineering, 9(4), 450–460. https://doi.org/10.1007/s11705-015-1542-2

Williams, J. L. (2001). Monolith structures, materials, properties and uses. Catalysis Today, 69(1), 3–9. https://doi.org/https://doi.org/10.1016/S0920-5861 (01)00348-0

Xu, C., Jiang, B., Liao, Z., Wang, J., Huang, Z., & Yang, Y. (2017). Effect of metal on the methanol to aromatics conversion over modified ZSM-5 in the presence of carbon dioxide. RSC Advances, 7(18), 10729–10736. https://doi.org/10.1039/c6ra27104a

Xu, L., Wu, S., Guan, J., Wang, H., Ma, Y., Song, K., Xu, H., Xing, H., Xu, C., Wang, Z., & Kan, Q. (2008). Synthesis, characterization of hierarchical ZSM-5 zeolite catalyst and its catalytic performance for phenol tert-butylation reaction. Catalysis Communications, 9(6), 1272–1276. https://doi.org/https://doi.org/10.1016/j.catcom.2007.11.018

Yan, Q., Doan, P. T., Toghiani, H., Gujar, A. C., & White, M. G. (2008). Synthesis gas to hydrocarbons over CuO-CoO-Cr2O 3/H+-ZSM-5 bifunctional catalysts. Journal of Physical Chemistry C, 112(31), 11847–11858. https://doi.org/10.1021/jp801640c

Zhu, Q., Takiguchi, M., Setoyama, T., Yokoi, T., Kondo, J. N., & Tatsumi, T. (2011). Oxidative dehydrogenation of propane with CO_2 over Cr/H [B] MFI catalysts. Catalysis Letters, 141(5), 670–677. https://doi.org/10.1007/s10562-011-0566-6.

II. 3D-PRINTED HZSM-5 AND 3D-HZM5@SAPO-34 STRUCTURED MONOLITHS WITH CONTROLLED ACIDITY AND POROSITY FOR CONVERSION OF METHANOL TO DIMETHYL EITHER

Fatima Magzoub, Xin Li, Shane Lawson, Fateme Rezaei, Ali A. Rownaghi*
Department of Chemical and Biochemical Engineering, Missouri University of Science and Technology, 1101 N State St., Rolla, MO 65409, United States
* E-mail: rownaghia@mst.edu

ABSTRACT

The ability to control the morphology and porosity of zeolite-structured monolith is an important step in the design of zeolite-based catalysts. Herein, additive manufacturing method was used for the rapid synthesis of HZSM-5 structured monoliths (3D-HZSM5) with hierarchical porosity (macro-meso-micro) and controlled type and density of acid sites. After 3D-HZSM5 monolith formation, the silicoaluminophosphate (SAPO-34) was grown on the 3D-HZSM5 structured monolith surface via secondary growth method for formation of 3D-HZSM5@SAPO-34 structured monolith. The samples were characterized before and after SAPO-34 growth by XRD, N_2 physorption, NH3-TPD, py-IR and SEM. The characterization results revealed formation of SAPO-34 layer on 3D-HZSM5 structured monolith and also modification also imply that formulation of H-ZSM-5 powder into monolith resulted in slightly less Brønsted acid sites while the density of Lewis acid sites increased. The performance of the 3D-HZSM5 and 3D-HZSM5@SAPO-34 structured monoliths were investigated in catalytic conversion of methanol to dimethyl ether (DME) over a temperature range of 180 to 320 °C for 10 h time on stream. The selectivity to DME was significantly increased as a result of modification in acidity and

porosity of the 3D-printed HZSM-5 structured monolith as compared to its powder counterpart and also 3D HZSM5@SAPO-34 structured monolith. SAPO-34 growth enhanced the density of strong acid sites which caused further conversion of DME to higher hydrocarbons. The highest DME selectivity reached 96% on 3D-HZSM5 structured monolith at 180 °C, which also achieved ~70% conversion of methanol.

Keywords: 3D printing, HZSM-5 monolith, Methanol dehydration, DME selectivity.

1. INTRODUCTION

Dimethyl ether (DME) has been receiving a growing attention as a clean alternative diesel fuel and precursor for production of a number of important chemicals such as light olefin, dimethyl sulfate, methyl acetate and is used as an aerosol propellant to replace chlorofluorocarbons (1,2). Traditionally, this has been accomplished via direct production from syngas or by one-pot methods, however, the high energy requirements and chemical waste outputs generated by these approaches make them extremely unattractive from both industrial and environmental standpoints. For these reasons, alternative means of DME production – such as catalytic DME production – have been studied in recent years.(3,4) Various metal catalysts and zeolites, such as HZSM, HY, RHO, SAPOs, SSZ-13 and γ-alumina have been studied for catalytic conversion of methanol to DME at temperatures around 180–400 °C (5–11). It is well known that methanol to hydrocarbon is a series of reactions by which methanol is first dehydrated to DME and water, followed by further formation of formation of C–C bonds such as light olefins and aromatics, from the C_1 oxygenate reactants (methanol or dimethyl ether) through hydrocarbon pool species(12).

According to the hydrocarbon pool mechanism, the higher alkenes and aromatics within zeolite cage will be methylated by C_1 oxygenate reactants and subsequently rearrangement that lead to the formation of alkyl side chains on the aromatic ring (13). However, alkyl aromatics in the product stream severely affects the performance of zeolite catalyst due to their favorable adsorption on active sites. Moreover, blocking micro-porous channels present in zeolite structure diminished the mass transfer through by imparting additional intraparticle diffusion resistance (14, 15). In addition, the alkyl aromatics are precursors to coke (i.e. carbonate) formation and subsequent catalyst deactivation. Therefore, the formation of active and stable secondary structures such as pellets, and extrudate honeycomb from nano or micrometer-sized zeolite particles remains a serious challenge for industrial applications (15, 16). In this regard, significant efforts have been made to increase the DME yield over zeolite catalysts by introduction of heteroatoms, such as ferrierite who exhibited reduce coking and enhanced water stability,(17,18) the SiO_2/Al_2O_3 ratio, alteration of particle size and porosity and fabrication of the structured catalyst(10,15,19,20).

Among different structured catalysts (e.g., pellets, beads, granules, or foams), structure monoliths with various types of interconnected or separated channels has have been proven to be excellent catalysts for chemical transformation and upgrading, as they impart enhanced mass transfer kinetics, especially from the bulk to the surface, as well as reduced pressure drops, which can diminish process energy costs (21–23). Conventionally structure monoliths are produced through extrusion process, however, extrusion molds must be manufactured to vary the structural geometry on a case-by-case basis. In turn, this drives up manufacturing costs and restricts the versatility of extruded monolith geometries

(24, 25). Recently, additive manufacturing method, or 3D printing, has emerged as a facile alternative to conventional extrusion, as it allows for digital customization of the as-manufactured scaffold, as well as high support loadings and retention of support properties (20,26–32). For example, Denayer and coworkers (33, 34) employed 3D-printing technique for preparation SAPO-34 and ZSM-5 monoliths for gas separation and also catalytic applications. Rezaei and coworkers (32, 35, 36) successfully prepared monoliths of porous materials like zeolites, aminosilicates, polymers and metal–organic frameworks (MOFs) and utilized them for various applications. The monoliths displayed excellent adsorption uptake comparable to that of powder sorbents and good mechanical integrity. Considering its significance in catalytic reactions, the study of 3D-printed monolithic zeolite catalyst is scarce. In this study, we developed a facile strategy to fabricate the self-supporting core–shell zeolite HZSM-5 structured monolith core and SAPO-34 shell grown on the surface of 3D printed HZSM-5 crystals. In this method, the 3D-printed HZSM-5 (3D-HZSM5) monoliths with honeycomb structures were first created and then subject to a hydrothermal SAPO-34 crystallization to obtain 3DHZSM5@SAPO-34 composite with nanosized SAPO-34 grown on the surface of each monoliths.

2. EXPERIMENTAL SECTION

2.1. FABRICATION OF 3D PRINTED HZSM-5 HONEYCOMB MONOLITHS

The physical characteristic of printing paste plays a critical role on the quality and structural integrity of 3D printed monoliths. The printing paste was prepared by mixing 87.5 wt. % HZSM-5 powders (Zeolyst, SiO_2/Al_2O_3 = 50), 10 wt. % bentonite clay powders

(Sigma-Aldrich), and 2.5 wt% methylcellulose using a roller for 3 h as powder. Then, ~10 mL of water was added to make the paste homogeneous and it was rolled for an additional 24 h at room temperature. Thereafter, it was densified using an agate mortar (Model IKA-R25) at 300 rpm and 50 °C until a printable rheology was observed. Then the printing paste was transferred into a syringe (Techcon Systems) carefully to prevent air voids and extruded through a Nordson 0.60 mm tip nozzle with a Nordson 0.60 mm in diameter on the syringe under a defined x-y-z route by computer. We used Simplify3D coupled with pronterface. The paste was dispensed and deposited on Teflon substrate in layer-by-layer manner to generate honeycomb-like monoliths. The 3D-prinetd HZSM-5 monoliths were noted as "3D-HZSM5". After drying at 100 °C under vacuum for 24 h, 3D-HZSM5 monoliths were subsequently calcined under air with a heating rate of 5 °C/min and kept at 550 °C for 5 h to remove the organic binders.

2.2. FABRICATION OF CORE–SHELL STRUCTURED 3D-HZSM5@SAPO-34 COMPOSITE

To obtain core–shell structured 3D-HZSM5@SAPO-34 composite, 3D HZSM5 monoliths were immersed in the water suspension of 1.0 wt. % SAPO-34 obtained seeds, and then were shaken gently for 5 min. SAPO-34 seeds were produced from a synthesis mixture of aluminum isopropoxide ($Al(i\text{-}C_3H_7O)_3$, Simga-Aldrich), colloidal silica (40 wt.%, SNOWTEX-ZL), tetraethylammonium hydroxide (TEAOH, 40 wt.%, Simga-Aldrich), and H_3PO_4 (85 wt.%, Simga-Aldrich) according to the literature (Xin Li, Rezaei, & Rownaghi, 2018). The seeded monoliths with the fresh solution mixture were transferred to the 100 mL Teflon-lined stainless steel autoclaves for hydrothermal treatment in a 200 °C, pre-heated convection oven, for 6 h. After synthesis, the autoclaves were removed from

the oven and were allowed to cool naturally at room temperature for 12 h. Finally, the obtained monoliths were washed with 100 mL deionized water (three times), dried overnight at 110 °C and calcined at 550 °C with a ramp rate of 5 °C/min for and held for 5 h to remove the template. The loading of SAPO-34 on 3D-HZSM5 (3D-HZSM5@SAPO-34) were ~ 5 wt. %. The loading of SAPO-34 was determined by measuring weights before and after crystal growth. Figure 1 shows the optical image of the 3Dprinted 3D-HZSM5 and 3D-HZSM5@SAPO-34 monoliths with two different diameters.

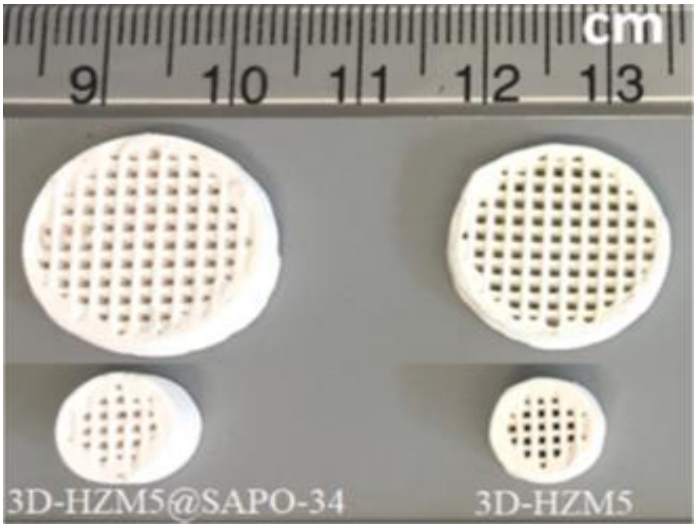

Figure 1. Optical image of the 3D-printed 3D-HZSM5 and 3D-HZsM5@SAPO-34 Monoliths

2.3. CHARACTERIZATIONS

The powder X-ray diffraction (PXRD) data were measured by PANalytical X'Pert Multipurpose X-ray Diffractometer operated at 40 kV and 40 mA with Cu-Kα1 (λ = 1.5418 Å) radiation, 2θ range of 5- 50°, and scan rate of 2.0° min^{-1}. Scanning electron microscopy (SEM, Hitachi S-4700) was used for collecting the morphologies of samples. The N_2

adsorption–desorption isotherms at 77 K were conducted by a Micromeritics 3Flex instrument after the samples were degassed at 350 °C under vacuum for 6 h. The textural properties (total surface area, external surface area, total pore volume, macropore volume, and micropore volume) of all materials were estimated by using Brunauer- Emmett-Teller (BET) equation and t-plot and Barrett-Joyner-Halenda (BJH) methods, respectively. The density and strength of acid sites were estimated by temperature-programmed desorption of ammonia (NH_3-TPD) using a Micromeritics 3Flex analyzer. The NH_3-TPD analysis were performed (after sample pretreatment) under a flow of 5 vol% NH_3/He at 100 °C to 600 °C with constant heating rate of 10 °C min^{-1}. The amount of desorbed NH_3 were measured by using mass spectroscopy (MKS instrument). The amount and ratio of Brønsted and Lewis acid sites were estimated by ex-situ pyridine-adsorption fourier-transform infrared spectroscopy (py-FTIR) using a Bruker Tensor spectrophotometer. All samples were activated at 400 °C for 4 h under vacuum to remove moisture and cooled down to 60 °C for adsorption of pyridine until saturation.

2.4. CATALYTIC EVALUATION OF METHANOL DEHYDRATION

The catalytic evaluations were carried out in a fixed-bed reactor containing a standard mass of catalyst (e.g., 0.50 g) at 180–320 °C and weight hourly space velocity (WHSV) of 2.6 $g.g^{-1}.h^{-1}$. Methanol concentration was controlled by introducing a flow rate of 30 mL/mi n of 99.5% N_2 through a methanol saturator. A K-type thermocouple was positioned in the center of the catalyst bed in order to monitor the temperature. The feed (N_2) was saturated with methanol (99.9%) in a bubble saturator at 30 °C. The structure temperature was maintained by a constant temperature bath. The inlet flow rate was

adjusted using a mass flow controller (MFC). The catalyst was then pretreated in situ at a heating rate of 10 °C/min under a flow of air (30 mL/min) and maintained at 500 °C for 2 h. The temperature was then decreased to the reaction temperature in flowing nitrogen. To avoid possible condensation of hydrocarbons, the temperature of the effluent line was constantly maintained at 80 °C. The products were analyzed on-line every 30 min using a gas chromatography (SRI 8610C) equipped with a flame ionized detector (GC-FID) connected to mxt-wax/mxt-alumina capillary column for hydrocarbons. Nitrogen was used as the carrier gas.

3. RESULTS AND DISCUSSION

3.1. CHARACTERIZATION OF CATALYSTS

The XRD patterns of all samples are displayed in Figure 2. Both HZSM-5 powder and 3D-HZSM5 monolith showed typical MFI framework characteristic peaks at 2θ = 7.96°, 8.88°, 23.2°, 23.3° and 24.0° corresponding to (101), (200), (501), (341) and (303) planes respectively(L. Xu et al., 2008). Additionally, the peaks at $2\theta = 9.7°$, 13.3° and 21.0° were observed on 3D-HZSM5@SAPO-34 and these peaks reflect the CHA framework of SAPO-34 crystal growth and are agreement with the patterns reported in literature (Z. Chen et al., 2018; Sun et al., 2014; Tan et al., 2002).

SEM images are presented in Figure 3 showing the morphology of the HZSM-5 powder and 3D-printed monoliths. Bulky agglomeration was observed by compression of the HZSM-5 powder and 3D-HZSM5 monolith which could be due to the use of binder and calcination of the bare monolith. The comparison between 3D-HZSM5, and 3D-

HZSM5@SAPO-34 monoliths indicated the successful growth of SAPO-34 crystal on 3D-HZSM5 monolith.

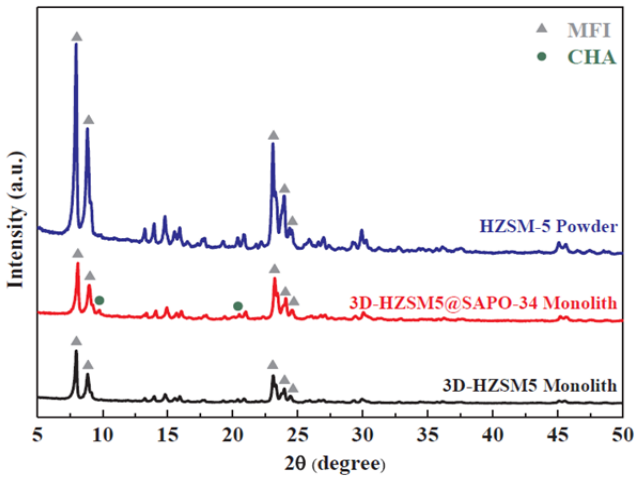

Figure 2. XRD patterns of the bare (3D-HZSM5, 3D-HZSM5/Silica) and SAPO coated (3D-HZSM5@SAPO-34, 3D-HZSM5/Silica@SAPO-34) 3D-printed monoliths.

After grown with, uniform SAPO-34 cubic crystals with average crystal size of ~3.4 μm with a thickness layer of ~5 μm were observed on 3D-HZSM5 monolith surfaces, which are marked with red frames in the cross sectional Figure 3c. and d. Notably, this further signified the formation of highly oriented crystals, which agreed with the XRD patterns. According to the weight measured before and after the shell growth, the SAPO-34 loading on 3D-HZSM5 monolith was about 5 wt. %. It is also worth noting here that, as shown in Figure 3d, the SAPO-34 growth was densely loaded throughout the zeolite surface and appeared to be homogeneous. Moreover, the size and structure of the SAPO-34 particles were comparable to those in established literature (i.e. cubic and ~ 3.4 μm) (38–40), indicating that the surface growth did not critically affect the SAPO-34 topology.

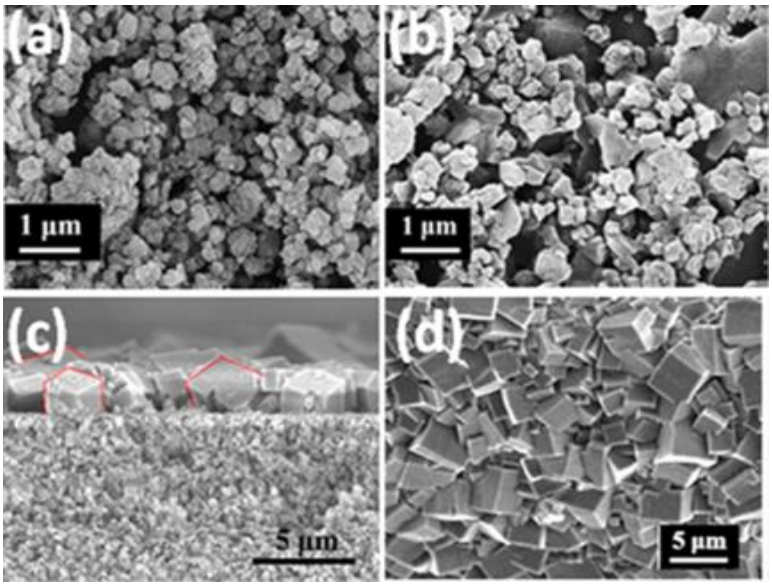

Figure 3. SEM images of the surface of (a) powder HZSM-5; (b) 3D-HZSM5; (c) 3D-HZSM5@SAPO-34; (d) top view of 3D-HZSM5@SAPO-34 monoliths.

As shown in Figure 4, all materials exhibited Type IV isotherms with hysteresis loop, which signify predominately mesoporous materials which also contain unfilled macropores (41). These isotherm and hysteresis profiles were to be expected, since H-ZSM-5 is a mesoporous material and burning out the plasticizer is a known method of generating macroporosity. Table 1 shows the textural properties of all the investigated samples. The comparison between HZSM-5 powder and 3D-HZSM5 monolith indicated that HZSM-5 catalyst underwent a decrease in total surface area from 429 $m^2\ g^{-1}$ to 373 $m^2\ g^{-1}$ after fabrication into the monolith. The comparison between the HZSM-5 powder and monoliths implies that the micropore volume decreased while mesopores volume increased after zeolite formulation into the monolith. This can be due to the addition of the less porous binder which diluted the zeolite and also creation of mesopores in the monolith by removal of the plasticizer after calcination. These results confirmed that the 3D-printing method, render the zeolite structured monolith with macro-meso-microprosity. Further

growth of SAPO-34-layer cause pore clogging and decrease both surface area and porosity of the 3D-HZSM5 monolith.

The acidity of the samples was analyzed with the NH_3-TPD and pyridine adsorption, as shown in Figure 5. The corresponding acid strengths and acid site densities are summarized in Table 2. As listed in Table 2, all samples show desorption of ammonia at 474–490 K (weak acid sites) and at 629–676 K (strong acid sites) (19, 37). As expected, the 3D-HZSM5@SAPO-34 monolith exhibited slightly higher total acid sites amount due to the introduction of acidic SAPO-34. The comparison between HZSM-5 powder and 3D-HZSM5 suggests that formulation of powder into monolith slightly decreased strong acid sites amount while the amount of weak acid sites increased simultaneously. As can be observed from these results, both the formulation into monolith structure and the further coating with CHA framework zeolite have significant effect on the catalyst acid strength distribution. The HZSM-5 powder exhibited slightly more total acid sites amount (ca. 0.58 mmol g^{-1}) compared to 3D-HZSM5 monolith (ca. 0.57 mmolg^{-1}) and less than 3D-HZSM5@SAPO-34 monolith (ca. 0.63 mmol g^{-1}). The formulation into monolith structure reduced the strong acid sites amount of HZSM-5 powder from 0.31 mmol g^{-1} to 0.20 mmol g^{-1} (3DHZSM5) and enhanced weak acid sites amount from 0.27 mmol g^{-1} to 0.36 mmol g^{-1}. The differences in acidity between the powder and monolith likely could be attributed to addition of the binder or may have also been caused by sintering between the zeolite particles reducing some of the site accessibility. The SAPO-34 growth on 3D-HZM5 increase strong acid sites from 0.20 mmol g^{-1} (3D-HZSM5) to 0.28 mmol g^{-1} (3D-HZSM5@SAPO-34).

Ex-situ py-FTIR analysis (Figure 4b) was used to better understand the type and density of the monolith's acid sites. The intensity of the IR band is proportional to the concentration of acid sites. According to previous studies (42,43), absorption appear at range of 1445–1460 cm^{-1} and 1540–1548 cm^{-1} are characteristic bands of Lewis (L) and Brønsted (B) acid site, respectively. All samples have shown bands around 1450 cm^{-1} and 1540 cm^{-1} and the density of corresponding Brønsted and Lewis acid sites are listed in Table 2, which imply that formulation into monolith resulted in slightly less Brønsted acid sites while the density of Lewis acid sites increased.

Table 1. Textural properties of zeolite samples.

Samples	S_{BET} [a] (m^2 g^{-1})	S_{micro} [b] (m^2 g^{-1})	S_{ext} (m^2 g^{-1})	V_{total} [c] (cm^3 g^{-1})	V_{micro} (cm^3 g^{-1})	V_{meso} (cm^3 g^{-1})
HZSM-5 powder	429	261	168	0.30	0.13	0.17
3D-HZSM5	373	214	159	0.30	0.13	0.20
3D-HZSM5@SAPO-34	336	206	130	0.27	0.10	0.17

[a] S_{BET} was obtained by analyzing nitrogen adsorption data at 77 K in a relative vapor pressure ranging from 0.05 to 0.30.
[b] Micropore area and micropore volume were determined using t-plot method.
[c] Total pore volume was estimated based on the volume adsorbed at P/Po = 0.99

3.2. CATALYST TESTS

The catalytic performance of all samples was evaluated in methanol to dimethyl ether reaction at four different temperatures (180–320 °C), space velocity of 2.6 $g.g^{-1}.h^{-1}$ for 10 h time-on-stream. The methanol conversion (X_{MeOH}) and DME selectivity results are shown in Figure 6. Over all samples, the methanol conversion enhanced by increasing reaction temperature. It can be observed that although HZSM-5 powder showed slightly

higher conversion than its monolith counterpart 3DHZSM5 at lower reaction temperature, but 3D-HZSM5 monolith was found to be active and stable at higher reaction temperature.

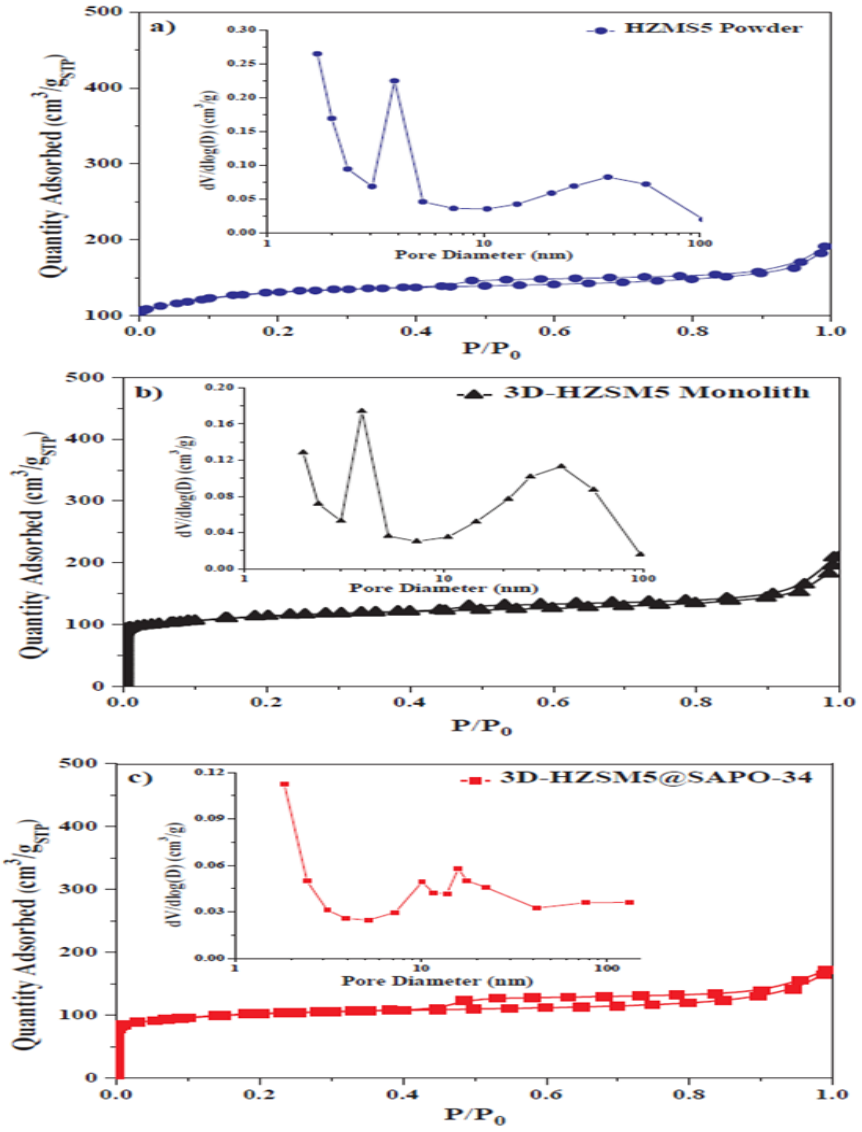

Figure 4. N_2 physisorption isotherms and PSD (insets) of (a) pure HZSM-5, (b) 3DHZSM5 and (c) 3D-HZSM5@SAPO-34.

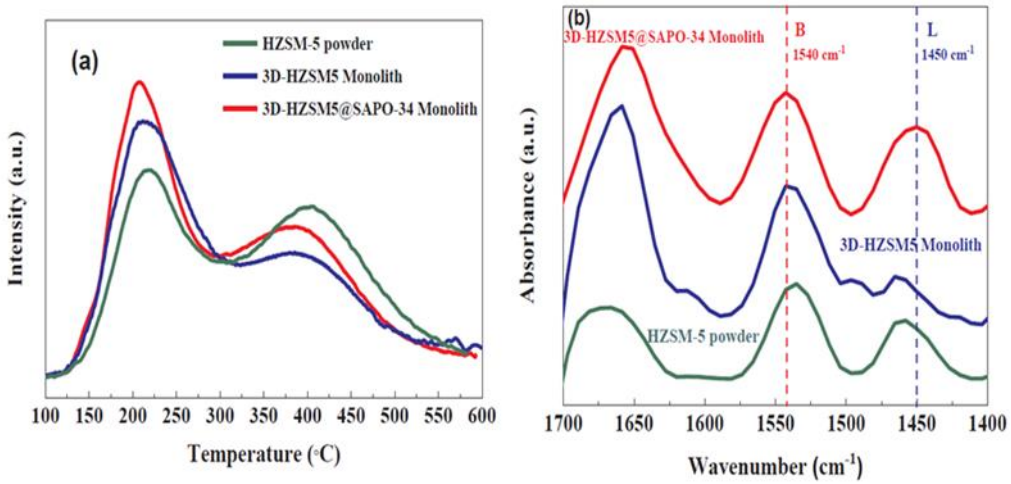

Figure 5. NH3-TPD profiles (a) and py-FTIR spectra (b) of the HZSM-5 powder, 3D-HZSM5, and 3D-HZSM5@SAPO-34 monoliths.

Table 2. Acid site distribution results calculated from NH_3-TPD profiles and pyridine adsorption.

Sample	Weak acid peak		Strong acid peak		L acid site	B acid site
	T (°C)	Amount (mmol g^{-1})[a]	T (°C)	Amount (mmol g^{-1})[a]	(mmol g^{-1})[b]	(mmol g^{-1})[b]
HZSM-5 powder	215	0.27	400	0.31	0.17	0.40
3D-HZSM5	213	0.36	377	0.20	0.19	0.38
3D-HZSM5@SAPO-34	210	0.35	380	0.28	0.22	0.41

[a] Total acid site amounts, weak and strong acid peak centers were obtained from NH_3-TPD profiles.
[b] Brønsted to Lewis site were calculated from pyridine adsorption FTIR bands intensity.

The lower methanol conversion over 3D-HZSM5 monolith might be the consequence of reduced site accessibility caused by sintering between the zeolite particles and inert binders during calcination, as previously discussed. This is in accordance with the acidic property results obtained from NH_3-TPD and py-FTIR measurements, where the

density of strong acid sites within the 3D-HZSM5 and 3D-HZDM5@SAPO-34 structured monoliths are lower than that of HZSM-5 powder. As reported previously (Jang et al., 2012), the zeolites with smaller crystallites exhibited higher catalytic activity due to higher availability of Brönsted acid sites within microporous and also higher reactant/product diffusivity.

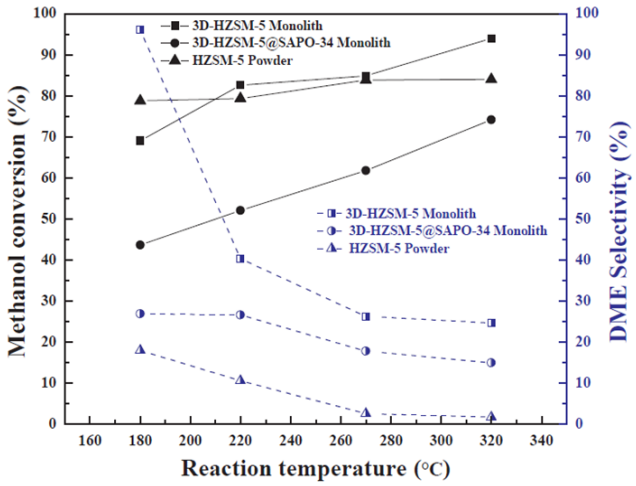

Figure 6. Methanol conversion (X_{MeOH}) and selectivity to DME as a function of temperature over HZSM-5 powder, 3D-HZSM-5, and 3D-HZSM-5@SAPO-34 monoliths. (10 h time-on-stream; WHSV: 2.66 $gg^{-1}h^{-1}$).

Overall, both monoliths exhibited higher selectivity towards DME than the HZSM-5 powder. Since it has been broadly accepted that DME is an intermediate and a precursor for formation of light olefins and other hydrocarbons within zeolite framework cages and channels it is proposed that the formulation of zeolite into the monolith structure. Furthermore, 3D-HZSM5@SAPO-34 shows slightly lower DME selectivity due to pore clogging which cause, lower porosity and surfaces area and intrazeolitic diffusion limitation which should be much severer in larger zeolite crystallites. Although the growth

of SAPO-34 on 3D-HZSM5 enhanced density of acid sites, however, it caused pore clogging which reduced microporous and mesopores size/volume dramatically, whereas both Brønsted and Lewis acid sites were increased by growth of SAPO-34 crystals. The 3D-HZDM5 showed higher methanol conversion and DME selectivity at all reaction temperatures because of its low number of strong Brönsted acid sites and higher micro/mesoporocity, shorter diffusion path allowing the rapid out diffusion of DME from 3D-HZDM5 catalyst monolith compared to 3DHZDM5@SAPO-34. The major products of the methanol conversion over both catalyst monoliths (3D-HZDM5 and 3D-HZDM5@SAPO-34) at 250 C were lower olefins such as ethylene and propylene, with very low formations of larger chain hydrocarbons and aromatics. At the same reaction conditions, DME yields over HZSM-5 powder after 120 min on stream were less than 5% because of its rapid deactivation and coke formation. The higher rate of coke formation over HZSM-5 powder was attributed to the further light olefin conversion to aromatics and paraffins as well as intrazeolitic diffusion limitation of larger hydrocarbons. These results are in agreement with previous report that confirmed HZSM-5/SAPO-34 composite with hierarchical structure is favored the conversion of methanol/DME to light olefins, larger hydrocarbons and aromatics (Dai et al., 2011; Hirota et al., 2010; Jang et al., 2012).

4. CONCLUSION

This work described the synthesis of 3D-printed HZSM-5, and 3DHZSM-5@SAPO-34 monoliths with a hierarchical (macro-meso-microporous) pore network. The formulation of 3D-HZSM5 structured monolith favored the mass transfer and DME

selectivity. The growth of SAPO-34 crystals via secondary growth method were applied to tune the porosity and acidity of 3D-HZSM-5 monolith. Catalytic evaluation of the zeolite monoliths in the methanol dehydration reaction indicated that the selectivity toward DME was favored 3D-HZSM-5 structured zeolite monolith. This study provides a foundation for preparation of zeolite monoliths with tunable properties by 3D printing method that can be tailored for specific chemical reactions.

DECLARATION OF COMPETING INTEREST

The authors declare that they have no known competing financial interests or personal relationships that could have appeared to influence the work reported in this paper.

ACKNOWLEDGEMENT

We thank the University of Missouri Research Board (UMRB) for supporting this work and Materials Research Center (MRC) of Missouri S&T for SEM and XRD.

SUPPLEMENTARY DATA

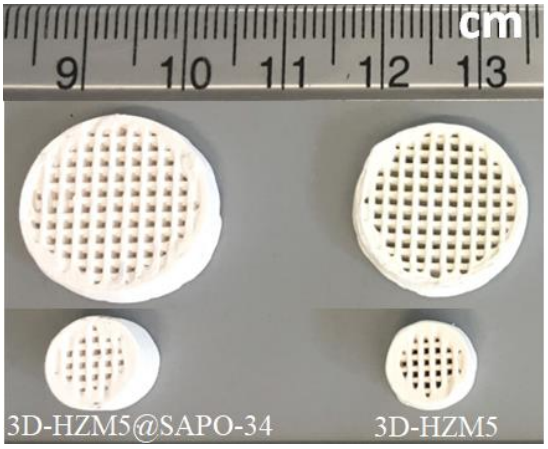

Figure S1. Optical image of the 3D-printed 3D-HZSM5 and 3D-HZsM5@SAPO-34 monoliths.

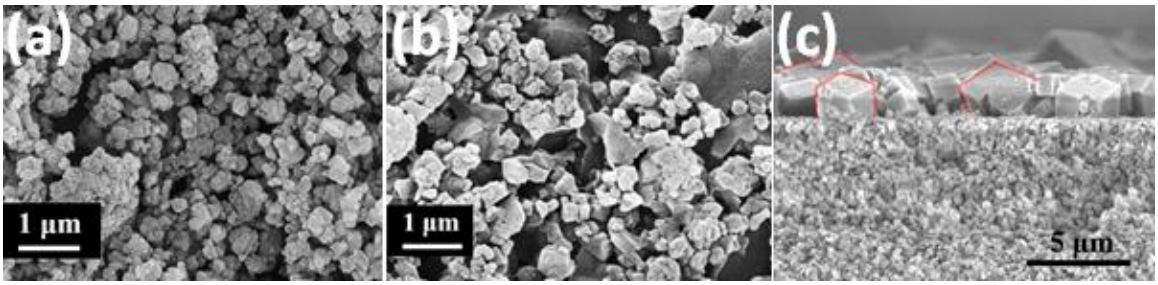

Figure S2. SEM images of the surface of (a) powder HZSM-5, (b) 3D-HZSM5, and (c) 3D-HZSM5@SAPO-34 monoliths.

REFERENCES

1. Unglert M, Bockey D, Bofinger C, Buchholz B, Fisch G, Luther R, et al. Action areas and the need for research in biofuels. Fuel. 2020;268:117227.

2. Mondal U, Yadav GD. Perspective of dimethyl ether as fuel: Part II- analysis of reactor systems and industrial processes. J CO2 Util [Internet]. 2019;32(xxxx):321–38. Available from: https://doi.org/10.1016/j.jcou.2019.02.006

3. Perathoner S, Centi G. CO2 recycling: A key strategy to introduce green energy in the chemical production chain. ChemSusChem. 2014;7(5):1274–82.

4. Catizzone E, Bonura G, Migliori M, Frusteri F, Giordano G. CO2 recycling to dimethyl ether: State-of-the-art and perspectives. Molecules. 2018;23(1):1–28.

5. Fei J, Hou Z, Zhu B, Lou H, Zheng X. Synthesis of dimethyl ether (DME) on modified HY zeolite and modified HY zeolite-supported Cu-Mn-Zn catalysts. Appl Catal A Gen. 2006;304(1–2):49–54.

6. Rownaghi AA, Rezaei F, Stante M, Hedlund J. Selective dehydration of methanol to dimethyl ether on ZSM-5 nanocrystals. Appl Catal B Environ [Internet]. 2012;119–120:56–61. Available from: http://dx.doi.org/10.1016/j.apcatb.2012.02.017

7. Khaleel A. Titanium-doped alumina for catalytic dehydration of methanol to dimethyl ether at relatively low temperatures. Fuel. 2011;90(7):2422–7.

8. Ladera R, Finocchio E, Rojas S, Busca G, Fierro JLG, Ojeda M. Supported WOx-based catalysts for methanol dehydration to dimethyl ether. Fuel. 2013;113:1–9.

9. Pinkaew K, Yang G, Vitidsant T, Jin Y, Zeng C, Yoneyama Y, et al. A new core–shell-like capsule catalyst with SAPO-46 zeolite shell encapsulated Cr/ZnO for the controlled tandem synthesis of dimethyl ether from syngas. Fuel. 2013;111:727–32.

10. Jin D, Zhu B, Hou Z, Fei J, Lou H, Zheng X. Dimethyl ether synthesis via methanol and syngas over rare earth metals modified zeolite Y and dual Cu–Mn–Zn catalysts. Fuel. 2007;86(17):2707–13.

11. Liu D, Yao C, Zhang J, Fang D, Chen D. Catalytic dehydration of methanol to dimethyl ether over modified γ-Al2O3 catalyst. Fuel. 2011;90(5):1738–42.

12. Huang J, Jiang Y, Marthala VRR, Bressel A, Frey J, Hunger M. Effect of pore size and acidity on the coke formation during ethylbenzene conversion on zeolite catalysts. J Catal. 2009;263(2):277–83.

13. Teketel S, Olsbye U, Lillerud K-P, Beato P, Svelle S. Selectivity control through fundamental mechanistic insight in the conversion of methanol to hydrocarbons over zeolites. Microporous Mesoporous Mater. 2010;136(1):33–41.

14. Rownaghi AA, Hedlund J. Methanol to gasoline-range hydrocarbons: Influence of nanocrystal size and mesoporosity on catalytic performance and product distribution of ZSM-5. Ind Eng Chem Res. 2011;50(21):11872–8.

15. Rownaghi AA, Rezaei F, Hedlund J. Yield of gasoline-range hydrocarbons as a function of uniform ZSM-5 crystal size. Catal Commun [Internet]. 2011;14(1):37–41. Available from: http://dx.doi.org/10.1016/j.catcom.2011.07.015

16. Tian P, Wei Y, Ye M, Liu Z. Methanol to olefins (MTO): From fundamentals to commercialization. ACS Catal. 2015;5(3):1922–38.

17. Sai Prasad PS, Bae JW, Kang S-H, Lee Y-J, Jun K-W. Single-step synthesis of DME from syngas on Cu–ZnO–Al2O3/zeolite bifunctional catalysts: The superiority of ferrierite over the other zeolites. Fuel Process Technol. 2008;89(12):1281–6.

18. Migliori M, Catizzone E, Aloise A, Bonura G, Gómez-Hortigüela L, Frusteri L, et al. New insights about coke deposition in methanol-to-DME reaction over MOR-, MFI- and FER-type zeolites. J Ind Eng Chem [Internet]. 2018;68:196–208. Available from: https://doi.org/10.1016/j.jiec.2018.07.046

19. Hoang TQ, Zhu X, Lobban LL, Resasco DE, Mallinson RG. Effects of HZSM-5 crystallite size on stability and alkyl-aromatics product distribution from conversion of propanal. Catal Commun. 2010;11(11):977–81.

20. Wang S, Bai P, Sun M, Liu W, Li D, Wu W, et al. Fabricating Mechanically Robust Binder-Free Structured Zeolites by 3D Printing Coupled with Zeolite Soldering: A Superior Configuration for CO2 Capture. Adv Sci. 2019;6(17):1–9.

21. Rezaei F, Webley P. Optimum structured adsorbents for gas separation processes. Chem Eng Sci [Internet]. 2009;64(24):5182–91. Available from: http://www.sciencedirect.com/science/article/pii/S0009250909005752

22. Ledesma C, Llorca J. CuZn/ZrO2 catalytic honeycombs for dimethyl ether steam reforming and autothermal reforming. Fuel. 2013;104:711–6.

23. Lam E, Luong JHT. Carbon materials as catalyst supports and catalysts in the transformation of biomass to fuels and chemicals. ACS Catal. 2014;4(10):3393–410.

24. Masala A, Vitillo JG, Mondino G, Martra G, Blom R, Grande CA, et al. Conductive ZSM-5-Based Adsorbent for CO2 Capture: Active Phase vs Monolith. Ind Eng Chem Res. 2017;56(30):8485–98.

25. Williams JL. Monolith structures, materials, properties and uses. Catal Today [Internet]. 2001;69(1):3–9. Available from: http://www.sciencedirect.com/science/article/pii/S0920586101003480

26. Li X, Alwakwak AA, Rezaei F, Rownaghi AA. Synthesis of Cr, Cu, Ni, and Y-Doped 3D-Printed ZSM-5 Monoliths and Their Catalytic Performance for n-Hexane Cracking. ACS Appl Energy Mater. 2018;1(6):2740–8.

27. Magzoub F, Li X, Al-Darwish J, Rezaei F, Rownaghi AA. 3D-printed ZSM-5 monoliths with metal dopants for methanol conversion in the presence and absence of carbon dioxide. Appl Catal B Environ [Internet]. 2019;245(September 2018):486–95. Available from: https://doi.org/10.1016/j.apcatb.2019.01.008

28. Li X, Rezaei F, Rownaghi AA. Methanol-to-olefin conversion on 3D-printed ZSM-5 monolith catalysts: Effects of metal doping, mesoporosity and acid strength. Microporous Mesoporous Mater. 2019;276(September 2018):1–12.

29. Li X, Rezaei F, Rownaghi AA. 3D-printed zeolite monoliths with hierarchical porosity for selective methanol to light olefin reaction. React Chem Eng. 2018;3(5):733–46.

30. Zhou X, Liu CJ. Three-dimensional Printing for Catalytic Applications: Current Status and Perspectives. Adv Funct Mater. 2017;27(30):1–13.

31. Lawson S, Adebayo B, Robinson C, Al-Naddaf Q, Rownaghi AA, Rezaei F. The effects of cell density and intrinsic porosity on structural properties and adsorption kinetics in 3D-printed zeolite monoliths. Chem Eng Sci [Internet]. 2020;218:115564. Available from: https://doi.org/10.1016/j.ces.2020.115564

32. Thakkar H, Lawson S, Rownaghi AA, Rezaei F. Development of 3D-printed polymer-zeolite composite monoliths for gas separation. Chem Eng J [Internet]. 2018;348:109–16. Available from: http://www.sciencedirect.com/science/article/pii/S1385894718307514

33. Couck S, Cousin-Saint-Remi J, Van der Perre S, Baron G V, Minas C, Ruch P, et al. 3D-printed SAPO-34 monoliths for gas separation. Microporous Mesoporous Mater [Internet]. 2018;255:185–91. Available from: http://www.sciencedirect.com/science/article/pii/S1387181117304869

34. Couck S, Lefevere J, Mullens S, Protasova L, Meynen V, Desmet G, et al. CO2, CH4 and N2 separation with a 3DFD-printed ZSM-5 monolith. Chem Eng J [Internet]. 2017;308:719–26. Available from: http://www.sciencedirect.com/science/article/pii/S1385894716312839

35. Thakkar H, Eastman S, Al-Naddaf Q, Rownaghi AA, Rezaei F. 3D-Printed Metal-Organic Framework Monoliths for Gas Adsorption Processes. ACS Appl Mater Interfaces. 2017;9(41):35908–16.

36. Lawson S, Al-Naddaf Q, Krishnamurthy A, Amour MS, Griffin C, Rownaghi AA, et al. UTSA-16 Growth within 3D-Printed Co-Kaolin Monoliths with High Selectivity for CO2/CH4, CO2/N2, and CO2/H2 Separation. ACS Appl Mater Interfaces. 2018;10(22):19076–86.

37. Xu L, Wu S, Guan J, Wang H, Ma Y, Song K, et al. Synthesis, characterization of hierarchical ZSM-5 zeolite catalyst and its catalytic performance for phenol tert-butylation reaction. Catal Commun. 2008;9(6):1272–6.

38. Chen Z, Li X, Xu Y, Dong Y, Lai W, Fang W, et al. Fabrication of nano-sized SAPO-11 crystals with enhanced dehydration of methanol to dimethyl ether. Catal Commun. 2018;103:1–4.

39. Tan J, Liu Z, Bao X, Liu X, Han X, He C, et al. Crystallization and Si incorporation mechanisms of SAPO-34. Microporous Mesoporous Mater. 2002;53(1):97–108.

40. Sun Q, Wang N, Xi D, Yang M, Yu J. Organosilane surfactant-directed synthesis of hierarchical porous SAPO-34 catalysts with excellent MTO performance. Chem Commun. 2014;50(49):6502–5.

41. Wacharasindhu S, Likitmaskul S, Punnakanta L, Chaichanwatanakul K, Angsusingha K, Tuchinda C. Serum IGF-I and IGFBP-3 Levels for Normal Thai Children and their Usefulness in Clinical Practice. J Med Assoc Thail. 1998;81(6):420–30.

42. Jang H-G, Min H-K, Lee JK, Hong SB, Seo G. SAPO-34 and ZSM-5 nanocrystals' size effects on their catalysis of methanol-to-olefin reactions. Appl Catal A Gen. 2012;437–438:120–30.

43. Meng X, Yu Q, Gao Y, Zhang Q, Li C, Cui Q. Enhanced propene/ethene selectivity for methanol conversion over pure silica zeolite: Role of hydrogen-bonded silanol groups. Catal Commun. 2015;61:67–71.

44. Dai W, Wang X, Wu G, Guan N, Hunger M, Li L. Methanol-to-olefin conversion on silicoaluminophosphate catalysts: Effect of brønsted acid sites and framework structures. ACS Catal. 2011;1(4):292–9.

45. Hirota Y, Murata K, Miyamoto M, Egashira Y, Nishiyama N. Light olefins synthesis from methanol and dimethylether over SAPO-34 nanocrystals. Catal Letters. 2010;140(1–2):22–6.

III. DESIGN AND SYNTHESIS OF GA, ZR, AND V-DOPED 3D-PRINTED ZSM-5 MONOLITHIC CATALYSTS FOR SELECTIVE FORMATION OF DME FROM METHANOL

Fatima Magzoub, Shane Lawson, Fateme Rezaei, Ali A. Rownaghi
Department of Chemical and Biochemical Engineering, Missouri University of Science and Technology, 1101 N State St., Rolla, MO 65409, United States
* E-mail: rownaghia@mst.edu

ABSTRACT

In this study, bifunctional catalysts (V_2O_5, ZrO_2, Ga_2O_3 doped H-ZSM-5) were synthesized through additive manufacturing method. The effect of direct metal oxide dpoing on HZSM-5 have been investigated in a continuous tubular microreactor at 200, 300, and 400 ℃, 1 bar, and a space velocity of 2.6 g/g.h.hr for methanol to dimethyl either (MTD) reaction. Characterization and correlation between the XRD, NH3-TPD, H_2-TPR, SEM-EDS and TGA/DTA experiments and the methanol dehydration activity revealed that the direct 3D printing of metal oxides combined with H-ZSM-5 can result in significant modification in the surface properties and bulk dispersion of the metal oxide phase, which in turn leads to a higher reducibility of the metal oxide doped HZSM-5 monolithic catalysts. Among the various compositions of metal oxides/H-ZSM-5, the 5 wt.% Ga/ H-ZSM-5 catalyst monolith exhibited the highest activity, achieving ~97% methanol conversion, ~40% dimethyl ether selectivity at 400 ℃. Overall, this study presents a novel way of manufacturing bifunctional structured catalysts which exhibit exceptional MTD performances.

Keywords: metal oxide, H-ZSM-5, methanol dehydration, DME, monolithic catalysts.

1. INTRODUCTION

Methanol-to-DME is one of the significant reactions in C1building block in the petrochemical industry and chemistry, the reaction offers an alternative cost-dynamic stand for producing DME as an alternative fuel (1). The properties of DME comparable to those of liquefied petroleum gases LPG but with more advantages such as roughly non-toxic, minimum NO_X emissions, lower smoke, and less engine noise, and because it turns into a liquid at room temperature it easier to store and transport and handle. (2–5).

DME) involved in several applications including a propellant in aerosol formulations as a basic material for the synthesis of dimethyl sulphate, methyl acetate, ethylidene diacetate, and light olefins (6, 7). Additional DME is a substitutional, neat, and friendly environment fuel for compression–ignition engines (8–12) and gas turbines (13), and a source of hydrogen for fuel cell applications (11, 14, 15). Furthermore, DME may use as a transporter for hydrogen.

Various solid acid catalysts such as zeolite (e.g., ZSM5, SAPO-34), metal oxides (e.g., γ-alumina, TiO_2, CeO_3) and bifunctional catalysts such as V_2O_5, ZrO_2, Cr_2O_3, Nb_2O_5, Mo_2C, Ga_2O_3 and In_2O_3 supported on metal oxides and or zeolites have been studied for their activity in the MTD reaction ; as these particular oxides provide the necessary active sites to reduce CO_2 into CO, while the support provides the acid surface sites necessary to dehydration of methanol into DME(4,17–20). These bifunctional catalysts are commonly synthesized and evaluated as powders and cannot be directly implemented into industrial reaction processes because high flow rates will lead to scattering and material loss (21, 22). Therefore, it is important to structure these bifunctional catalytic materials prior to

utilization in MTD reaction. One way to accomplish this at the millimeter scale is by 3D printing them into honeycomb monoliths. This technique is especially attractive from an industrial perspective, as it allows the as-manufactured scaffold's geometry to be digitally tuned without necessitating the production of extrusion molds, thereby reducing machining, labor, and material costs (26–28).

In our previous works, we developed zeolite/oxide catalysts for methanol-to-olefin conversion by 3D printing. However, the incipient impregnation technique, where nitrated metal salts were dissolved in the printing paste and calcined to form the oxide components, produced hydrophobic binding behavior and non-flowing rheology upon increasing the oxide loading beyond 5 wt.%. Because of this, the conversion of methanol to propylene was previously limited to further convention of DME to light olefins and aromatics. The most obvious way of addressing these low conversions would be to increase the oxide concentration within the scaffold, thereby enhancing the number of oxidation states during reaction and increasing the surface density of active sites on the oxide component. However, this cannot be accomplished by the impregnation approach, on account of the aforementioned hydrophobic behavior. For this reason, a new method to increase the oxide loading whilst maintaining a favorable rheology must be developed to enhance the catalytic properties of 3D-printed H-ZSM-5/oxide monoliths.

Motivated by this exciting possibility, this study reports the direct formation of oxide/HZSM-5 bifunctional structured catalysts with high oxide loading (single and mixed-metal oxide) through additive manufacturing method by directly printing insoluble metal oxides alongside H-ZSM-5 within a single ink. This method for formation of bifunctional heterogeneous catalyst offers an effective strategy to develop superior MTD

with not only high selectivity but also high activity that could be used to manufacture various bifunctional structured catalysts by incipient impregnation and calcination using nitrate salts. As such, the new additive manufacturing method reported herein opens up novel and important pathways through which 3D-printed structured heterogeneous catalysts can be customized.

The objectives of this investigation are to understand the additional influence of a Ga, Zr or V promoter on a HZM-5 bifunctional catalyst with respect to the high catalytic performance and stability for a single-step synthesis of DME from methanol at 200-400 °C.

2. EXPERIMENTAL

2.1. MATERIAL AND FEED

All materials applied in this work from Sigma Aldrich (Ga_2O_3 (99.99%), ZrO_2 (99%), V_2O_5 (98%), bentonite clay (Sigma), and methylcellulose (99%). The H-ZSM-5 was synthesized from the calcination of commercial ammonia-ZSM-5 powder (CBV 5524G, Zeolyst, SiO_2/Al_2O_3 = 50) at 823 K for 6 h.

The feed (Methanol 99.9%) was purchased from Fisher Scientific and all UHP gases from Airgas.

2.2. PASTE OXIDE RATIO AND 3D-PRINTING FORMULATION STEPS

All catalysts were synthesized as 3D-printing monoliths. The metal oxides were added as a powder to ZSM 5 to manufacturing the monoliths. The ratio for all metal oxides was kept the same (4%) balanced with HZSM5.

The paste fabrication details and ratio components in Table 1 were 3D-printed into the steps for 3D-printing manufacturing setup particularly in previous work (24, 29–32). The weight ratio from Table 1 for metal oxide and HZM5 and bentonite clay were mixed inside of a PTFE bottle with 15 mL of DI water. The bottle was well shaken and the mixture was rolled at 30 rpm for 48 h at room temperature in Roller. The slurry was formed after transferring the mixture to a PTFE beaker located in the touch of the ultrasonic bath and stirred it after added the weight % of methylcellulose listed in table 1. The same step for 3D-printing was followed as mention earlier. After printing, the monoliths were dried overnight at 25 °C. Then the monoliths were calcined at 550 °C for 6 h.

Table 1. Paste compositions used for manufacturing the catalyst monoliths.

Catalysts Name	**Ga_2O_3 (wt. %)**	**ZrO_2 (wt. %)**	**V_2O_5 (wt. %)**	**HZSM 5 (wt. %)**	**Bentonite clay (wt. %)**	**Methylcellulose (wt. %)**
ZSM5 Bare	0	0	0	84.8	12.7	2.5
4%Ga/ZSM5	3.4	0	0	81.4	12.7	2.5
4%(GaZr)/ZSM5	3.4	3.4	0	78	12.7	2.5
4%(GaV)/ZSM5	3.4	0	3.4	78	12.7	2.5

2.3. CHARACTERIZATION

The X-ray diffraction (XRD) patterns were run to analyze the crystallography of the sample and performed by using a PANalytical X'Pert multipurpose X-ray diffractometer with a scan step size of 0.02°/step at the rate of 137.2 s/step from $5 < 2\theta <$

90 °. The samples' physisorption properties were evaluated by N_2 adsorption measurements at 77 K on a Micromeritics (3Flex) gas analyzer. Before analysis, the samples were degassed under vacuum at 350 °C on a Micromeritics Smart VacPrep system for 6 h. The surface area and pore volume were calculated by the Brunauer-Emmet-Teller (BET) and non-local density functional theory (NLDFT) methods, respectively. The diffractive patterns were collected using zero-noise silicon substrates (SIL'TRONIX). The surface topographies were assessed by high-performance field emission scanning electron microscopy (FE-SEM) on a Zeiss Merlin Gemini microscope. Energy dispersive spectroscopy (EDS) was collected on a Bruker 5030 X-Flash diffractometer using an accelerating voltage of 25 kV. NH_3-TPD and H_2-TPR were both performed on 3Flex using a method that was outlined in our previous works (33, 34).

2.4. CATALYTIC TEST

The catalytic assessment was carried out in a fixed-bed reactor containing a standard mass of catalyst (e.g., 0.50 g) at 200, 300, and 400 °C and weight hourly space velocity (WHSV) of 2.6 g/g.h. Methanol fed to the reactor by inserting N_2 (99.5%) through a methanol saturator at 30 °C and adjust the flow rate at 30 mL/min by a mass flow controller (MFC). A K-type thermocouple was positioned in the center of the catalyst bed to monitor the bed temperature. The structure temperature was maintained by a constant temperature bath. The catalyst was then pretreated in situ at a heating rate of 10 °C/min under a flow of air (30 mL/min) and maintained at 500 °C for 2 h. The temperature was then decreased to the reaction temperature in flowing nitrogen. To avoid possible condensation of hydrocarbons, the temperature of the effluent line was constantly

maintained at 80 °C. The products were analyzed on-line every 30 min using gas chromatography (SRI 8610C) equipped with a flame ionized detector (GC-FID) connected to mxt-wax/mxt-alumina capillary column for hydrocarbons. Nitrogen was used as carrier gas.

3. RESULTS AND DISCUSSION

3.1. XRD ANALYSIS

The XRD patterns for all monoliths are shown in Figure (1). The peaks observed at $2\theta = 8.0$, 9.0, 14.8, 22.9, 24.0 and 29.8°, are corresponding to, (101), (200), (301), (501), (303), and (503) planes, respectively, in each of 4%GaZSM5, 4%(GaZr)ZSM5, and 4%(GaV)/ZSM5 which agreed with MFI structure and indicate the ZSM5 structure kept same even after incorporating with metal oxides (35)(36). As evident, the gallium, zirconium, and vanadium oxide monoliths exhibited diffractive indices which were consistent to those for ZSM-5. The peaks observed for all samples contain Gallium at 2θ = 22° which is attributed to the (201) plain of Gallium oxide rod (37). For 4 %(GaZr)/ZSM5 has diffraction peaks at 2θ = 28.2°, 31.5°, and 38.5°, which are corresponding, to [−111], [111], and [120] planes, respectively index of nanoscale ZrO_2. (38, 39). Additionally, the intensity is less due to Gallium which is a sign of high Gallium distribution on the surface. Noting, 4 %(GaV)/ZSM5 have a peek at $2\theta = 22^{o}$ which is related to the (001) index of crystalline V_2O_5 (34).

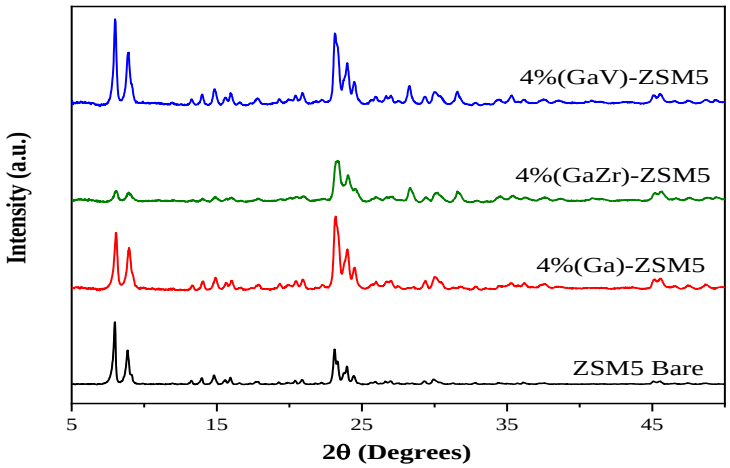

Figure 1. XRD patterns of bare and metal oxide-doped HZSM-5 monoliths.

3.2. TEXTURAL PROPERTIES

The textural properties of the monolith catalysts and pore distributions were specified by N_2 physisorption isotherms which are presented in Figure 2 and summarized in Table 2. It can be noted that all the monoliths behaved similarly to type IV physisorption, which is presented by mesoporous adsorbents and somewhat similar to H4 hysteresis loop which is consistent with microporous and mesoporous zeolites such as H-ZSM-5 and indicated that neither the 3D-printing method nor the calcination step significantly changes the pore structure (42).

Table 2. concludes the textural properties of the tested 3D-printed monolithic catalysts. Compared with the HZSM5 powder from the previous work (31,34) all monoliths subjected a decrease in total surface area and pore volume that were be expected as they are consistent with the oxide and bentonite concentrations within the 3D-printed monolithic catalysts.

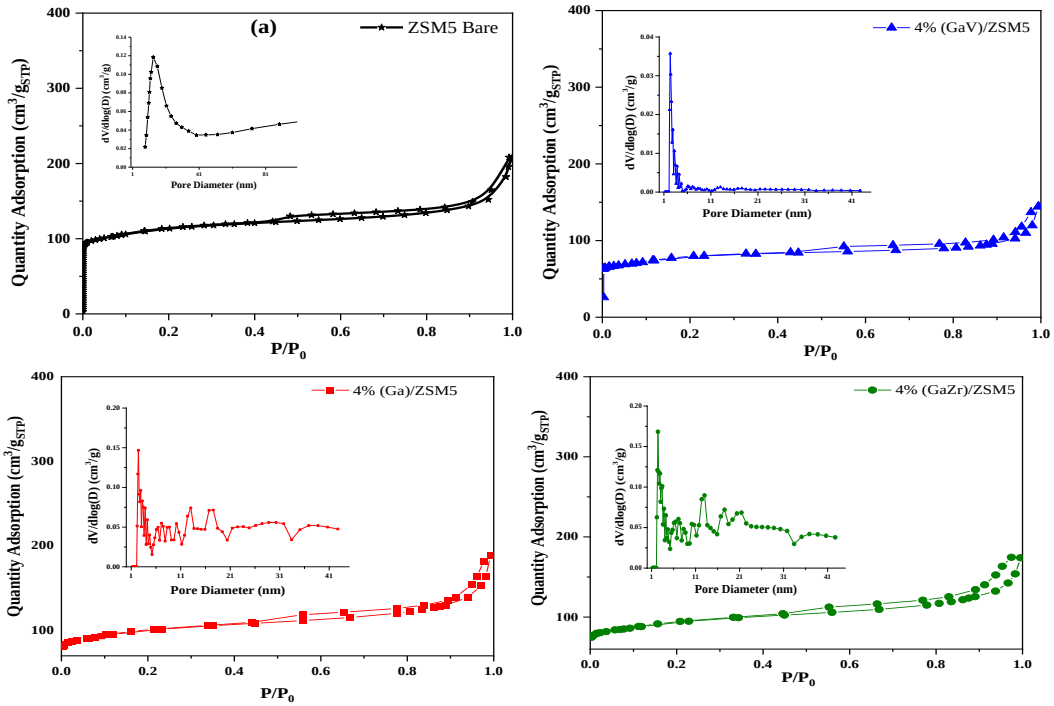

Figure 2. N_2 physisorption isotherms and pore distributions (insets) for bare and metal oxide-doped HZSM-5 monoliths.

Table 2. Textural properties of the 3D-printed oxide@ZSM-5 catalyst monoliths.

Monoliths Name	S_{BET} (m^2g^{-1})[a]	V_{total} (cm^3g^{-1})[b]	Pore D
ZSM5 Bare	373	0.30	2.5
4%Ga/ZSM5	321	0.24	1.58, 1.48, 1.4
4%(GaZr)/ZSM5	303	0.21	1.58, 1.84
4%(GaV)/ZSM5	256	0.20	1.58

[a] S_{BET} was obtained by analyzing nitrogen adsorption data at 77 K in a relative vapor pressure ranging from 0.05 to 0.30.
[b] Total pore volume was estimated based on the volume adsorbed at P/Po = 0.99.

3.3. MORPHOLOGIES AND ELEMENTAL MAPPING

Figure 3 shows scanning electron microscopy (SEM) of 4%Ga/ZSM5 and gallium mapping. In Figure (3a), the monoliths exhibited channels that were ~300 µm in diameter

and showed no visible cracking. The surface topographies were rough and contained pores of ~5-10 µm in diameter, which were likely formed during methylcellulose removal (Figure 3b-3c). (43). It worth observing that in the red arrow (Figure 3c), a brief bar-like structure was detected across the monolith surface. After zooming in (Figure 3d), was found to be ~5 µm in diameter. Using EDS was identified as gallium oxide (Figure 3e-3f). The literature agreed with that (44).

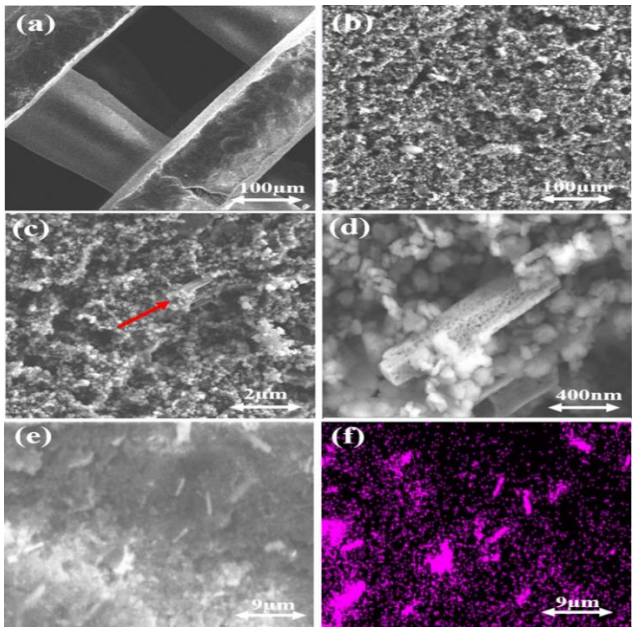

Figure 3. SEM images of the surface of 4%Ga/ZSM-5, (a-d) SEM micrographs, (e-f) Gallium maps.

Figure 4 shows scanning electron microscopy (SEM) of 4 %(GaZr)/ZSM5 and (gallium, Zirconium) mapping. As presented in Figure 4a, the channels of the monolith uncloudy and the diameter was approximately 500 µm. Also, slight cracking was observed (Figure 6a). The crack caused for the same reason as on 4%Ga/ZSM5. The surface topographies were rough (Figure 4(b,c)), it has been noting also in figure 4d tetrahedral

structure was appeared and that refers to tetragonal ZrO_2 or t-ZrO_2 which is consisted from the affected of Ga_2O_3 on ZrO_2.(45)(46). XRD results proved the ZrO_2 appearance. Looking at Figure (4e, 4f) the distribution of gallium oxide exhibited all over the crystallite surface. On the other side, the zirconium oxide is distributed heterogeneously Figure (4e, 4g).

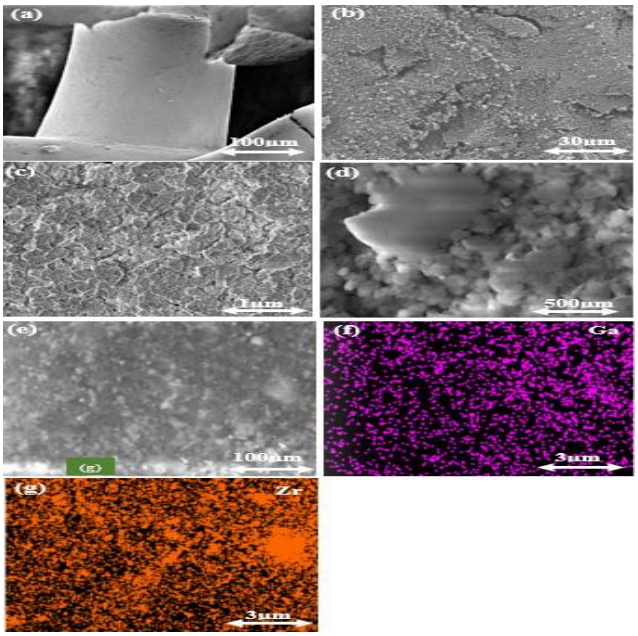

Figure 4. SEM images of the surface of 4 %(GaZr)/ZSM-5 (a-d) SEM micrographs, (e.f) gallium, (e.g) Zirconium maps.

The SEM images and vanadium map for 4%GaV@ZSM-5 are shown in Figure 5. From Figure 5a, the monolith exhibited cracking. Notably, this was not observed in the previous sample and may have been caused by the chemical interactions between vanadium oxide and zeolite during calcination. Namely, the reformation of the zeolite bonds could have led to additional gas generation during heating, thereby introducing surface flaws. A similar impact was occurred in (43). While the overall structure was stable. In the higher magnification images, a cluster phase distribution with some collapse in the surface was

observed in Figure 5b. Upon zoom in one of these areas (Figure 5c), two structures phases were clarified. First a bar-like structure identified as Ga_2O_3 exhibited in 4%GaZSM5. Second in figure 5d is pentagonal-structure is refer to vanadium-substituted H-ZSM-5 particles (47). Looking at figure (5e, 5f) the distribution of gallium oxide exhibited heterogeneously on the surface. However, a high distribution of the vanadium oxide appeared in the surface Figure (5e, 5g).

3.4. REDUCIBILITY OF 3D PRINTING MONOLITHS

The results appeared in Figure 6 is to exhibit the H_2-TPR of all 3D-Printing monoliths. Two different peaks demonstrate among most of the monoliths which demonstrate the probability of two reduction steps for metal species. For 4%Ga/ZSM5 the small reduction peak appeared at a lower temperature 150°C explained the appearance of low dispersed gallium oxides on the external surface which can be reduced at low temperature that's agreed with the SEM results. The second reduction peak observed at 650°C for the same monolith corresponds to the reduction of Ga2O3 to Ga2O joined into the ZSM5 framework (48).

Additionally, for 4%(GaV)/ZSM5 the reduction peaks illustrate at range 500-600°C assign to the reduction phenomenon of V_2O_5 to V_6O_{13} then the formation of V_2O_3 by the reduction of V_2O_4 (49,50). At low temperature, the redox behavior of all bimetallic monoliths observed in the range of (150 – 250 °C). Overall, depending on the results of H_2-TPR the reducibility of ZSM 5 has been changed due to the reduction behavior of the metallic oxide.

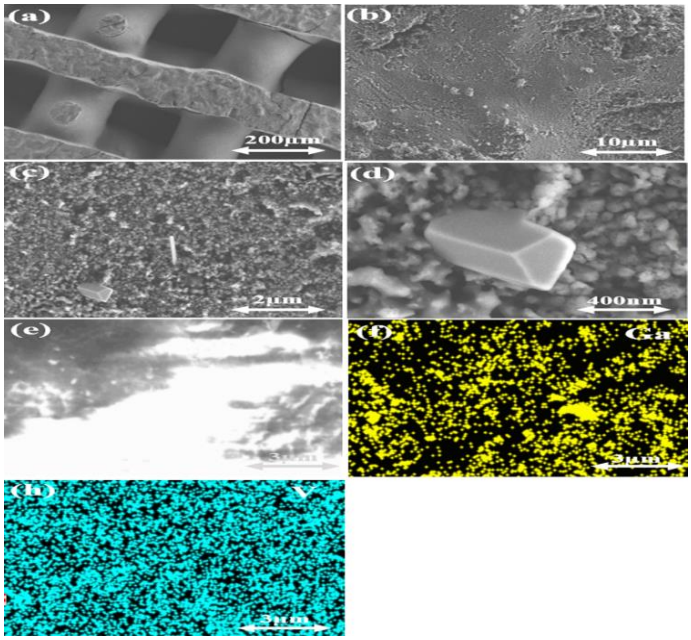

Figure 5. SEM images of the surface of 4 %(GaV)/ZSM-5, (a-d) SEM micrographs, (e.f) gallium, (e.g) Vanadium maps.

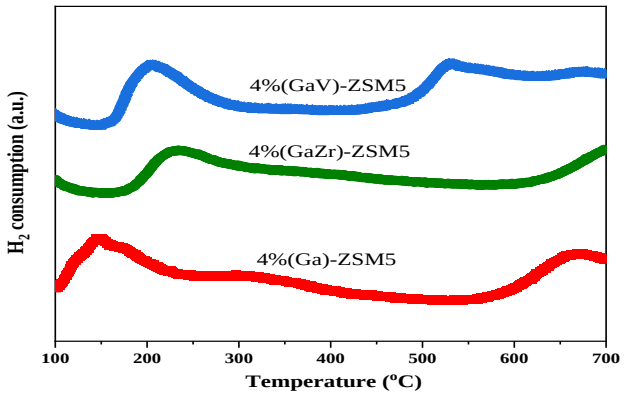

Figure 6. H_2-TPR profiles of all the 3D-printing monoliths.

3.5. THE ACIDITY OF 3D-PRINTING MONOLITHS

The temperature-programmed desorption of ammonia (NH_3-TPD) experiments in Figure 7 was carry out to display the acidic properties of all the Monoliths. High-intensity peaks in the range of (100−250 ° C) has been observed for all the monoliths symmetric to

the week aside side. Depend on the literature for the bare ZSM-5, double peaks should be found, refer to weak acid side and strong acid side (35, 51, 52). So the losses in the strong peak on the monoliths indicating that the structure of the ZSM5 change. An extra peak exhibited in 4%Ga/ZSM5 with small intensity in the range of (300−450°C) that refers to a strong acid side. The behavior of gallium in zeolite ZSM-5 minimizes the intensity of acidic sites and generates gallium species outside the network that can increase the methanol dehydration to DME (51).

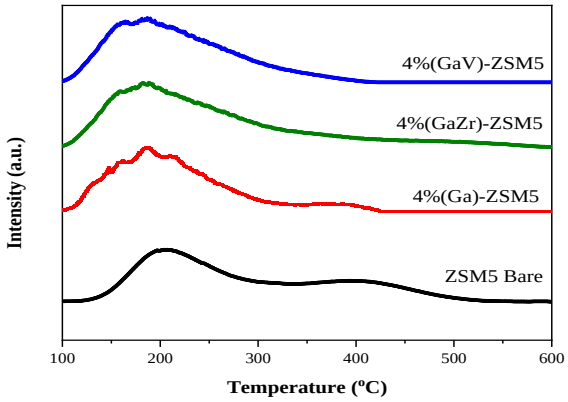

Figure 7. NH_3-TPD profiles of all the 3D-printing monoliths, bare ZSM5, 4 %(Ga)/ZSM5, 4 %(GaZr)/ZSM5 and 4 %(GaV)/ZSM5

3.6. CATALYSTS PERFORMANCE

The catalytic behavior of all monoliths has been investigated in methanol to dimethyl ether reaction at temperatures (200, 300, and 400 °C), the space velocity of 2.6 g/g.h for 10 h time-on-stream. The results visualized in Figure 11 indicated the methanol conversion (X_{MeOH} (%)) and the selectivity toward DME (S_{DME} (%)) for all the monoliths. All the catalysts indicated high methanol conversion with temperature increase but the DME selectivity it mutates between monoliths, due to the different acidic and metallic

properties. The results from the catalysis stability experiments at 200-400 °C are shown in Figure 11. The highest DME selectivity (~80%) was obtained with the bare HZSM-5 at 200 C and Ga@ZSM-5 monoliths at 300 and 400 C, while methanol conversion of ~85%, ~90 and ~97% were obtained over Ga@ZSM-5 monoliths at all reaction temperatures.

In the case of monometallic catalyst (4%Ga/ZSM5) the DME selectivity even at high temperature up to 400°C enhanced most likely due to the decrease in the strong acid site (Bronsted acid side) of the HZSM5 and shifted to weak Lewis acid sites led to hinder side reaction (53) and as another evidence all the peaks below 250°C signifying to Lewis acid site (54). On the other hand, the bimetallic catalysts (4 %(GaZr)/ZSM5, and 4 %(GaV)/ZSM5, represented decrees in DME selectivity with increasing the reaction temperature due to the formation of other hydrocarbons and coke formation. In general, the monometallic catalysts achieved higher activity as well as higher deactivation contrasted to the bimetallic catalysts (55).

Table 3 presented the methanol conversion and the product selectivity for all the monoliths in the three-reaction temperature. It worth noting that the highest DME selectivity (and a lower amount of other hydrocarbons such as methane, olefins, aromatics, and BTX are obtained at the lower reaction temperature, while higher methanol conversion is favor at the higher temperature (e.g., 400 °C). On the basis of these results, the oxide/zeolite catalysts' activities were concluded as Ga@ZSM-5 showed the highest methanol conversion at all reaction temperatures and also higher DME selectivity above 300 °C. The facile reducibility of Ga2O3 particles with high dispersion and an appropriate acidity and electronic state of Ga species are mainly responsible for the superior catalytic performance with the help of structural promoting effects of Ga promoters on ZSM-5.

In comparison to an unpromoted bifunctional catalyst, promoted catalysts with both Ga-Zr and Ga-V showed a higher catalytic performance and stability at 200 and 300 °C, however, both monolithic catalysts were deactivated at higher temperature of 400 °C due to coke formation.

Table 3. Methanol conversion and DME selectivity results through different temperature and overall monoliths

Monoliths	Reaction Temperature (°C)	Methanol conversion (%)	Selectivity (%)	
			DME	Other HCs
ZSM5 Bare	200	69.16	80.64	19.36
4%(Ga)/ZSM5	200	85.21	73.9	26.10
4%(GaZr)/ZSM5	200	81.92	24.98	75.02
4%(GaV)/ZSM5	200	81.42	32.28	67.72
ZSM5 Bare	300	81.07	25.03	74.97
4%(Ga)/ZSM5	300	90.47	38.99	61.01
4%(GaZr)/ZSM5	300	84.08	24.56	75.44
4%(GaV)/ZSM5	300	82.46	30.28	69.72
ZSM5 Bare	400	86.83	19.96	80.04
4%(Ga)/ZSM5	400	96.49	38.64	61.36
4%(GaZr)/ZSM5	400	71.41	1.13	98.87
4%(GaV)/ZSM5	400	62.69	2.93	97.07

3.7. THERMOGRAVIMETRIC ANALYSIS-DIFFERENTIAL THERMAL ANALYSIS (TGA-DTA)

The weight loss profiles from TGA for the monoliths following reaction are shown in Figure 9. At reaction temperature 200°C the weight loss for all the monolith <2% suggesting that the effect on coking may be minimal at this temperature. At reaction temperature 300°C, all monoliths shown weight loss at the rang (200 -300°C), Ga@ZSM-

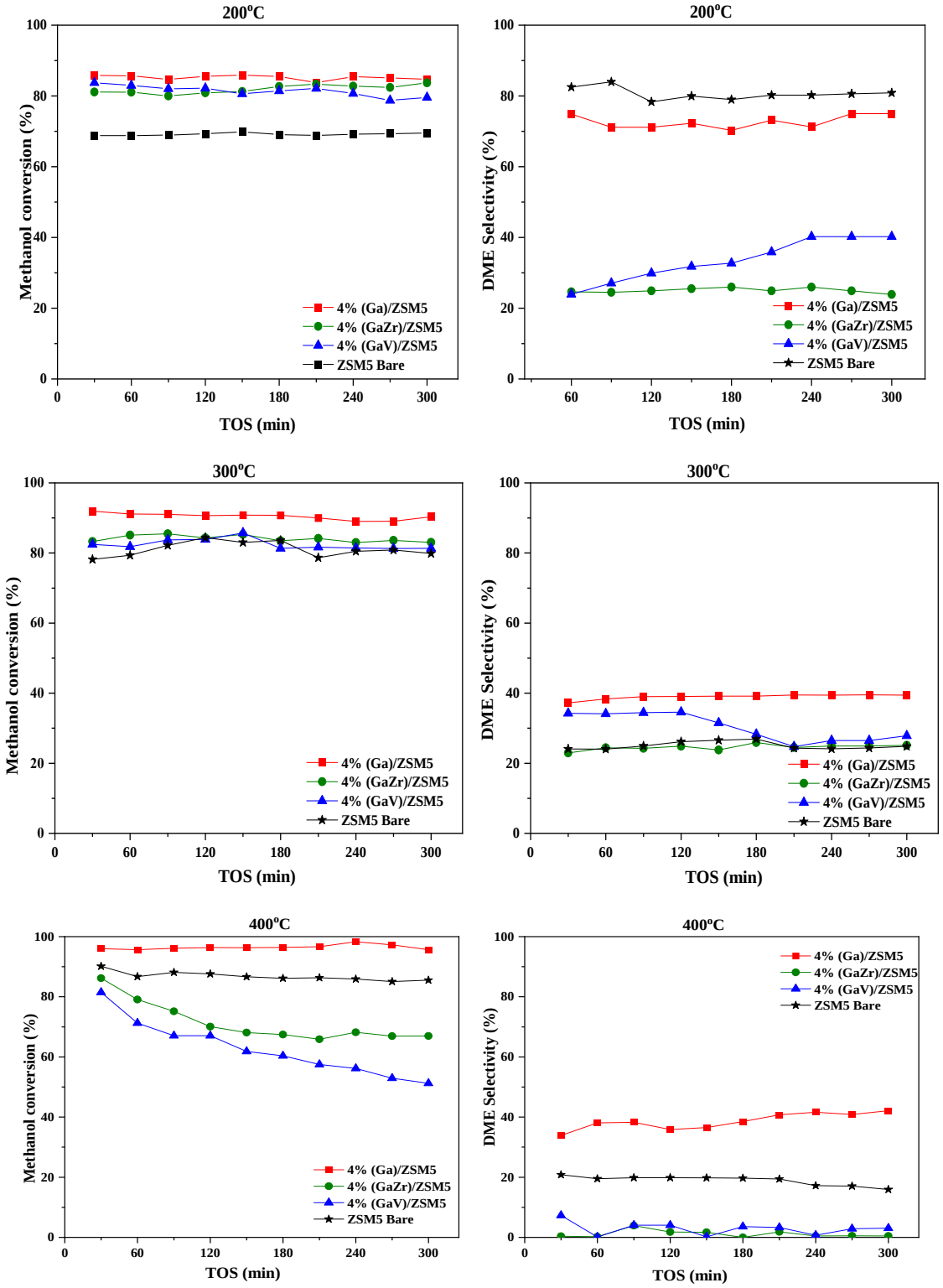

Figure 8. Test of bare ZSM5, 4 %(Ga)/ZSM5, 4 %(GaZr)/ZSM5, and 4 %(GaV)/ZSM5 for Methanol conversion (%) and selectivity to DME as a function of Time on stream (TOS). (WHSV= 2.66 $gg^{-1}h^{-1}$).

5 exhibited 2.7% weight loss, but 2.07% and .87% weight loss by addition of Zr and or V to Ga respectively. Beside the weight loss at 500°C > the weight loss decrease to be 2.1% for Ga-ZSM5, 0.7% for GaZr-ZSM5, and 0.2% for GaV-ZSM5 in other way the coking amounts were nearly identical for all the monoliths, further suggesting that this new method produces monoliths which are highly stable.

However, at reaction temperature 400°C substantial differences were observed between GaZr-ZSM5 and GaV-ZSM5 with 10.6% and 11.9% respectively, in compared to Ga-ZSM5 and bare ZSM5 which they shown <1.3% for both. Overall, the coking amounts across all samples were significantly less than monoliths produced by the wet-impregnation technique in our previous work (30).

4. CONCLUSION

This work demonstrated a novel method of manufacturing high-loaded catalyst monoliths for MTD reaction through direct 3D-printing of insoluble oxides. All catalyst monoliths displayed here showed favorable performance in MTD, where the best performance was observed in the Ga@ZSM-5, which produced an 85% methanol conversion as well as nearly 74% DME selectivity. Given that this work demonstrated a proof-of-concept for this new technique, without any optimization regarding calcination temperature, zeolite/oxide loadings, and monolith geometry, we anticipate that these materials can be further tuned to enhance the methanol conversion, DME, and light olefins selectivity. Overall, this work has demonstrated an extremely effective and versatile means of manufacturing 3D-printed catalysts that outperform the current state-

of-art materials, such as monoliths produced with nitrate impregnation, where propane conversion was limited to 5%.

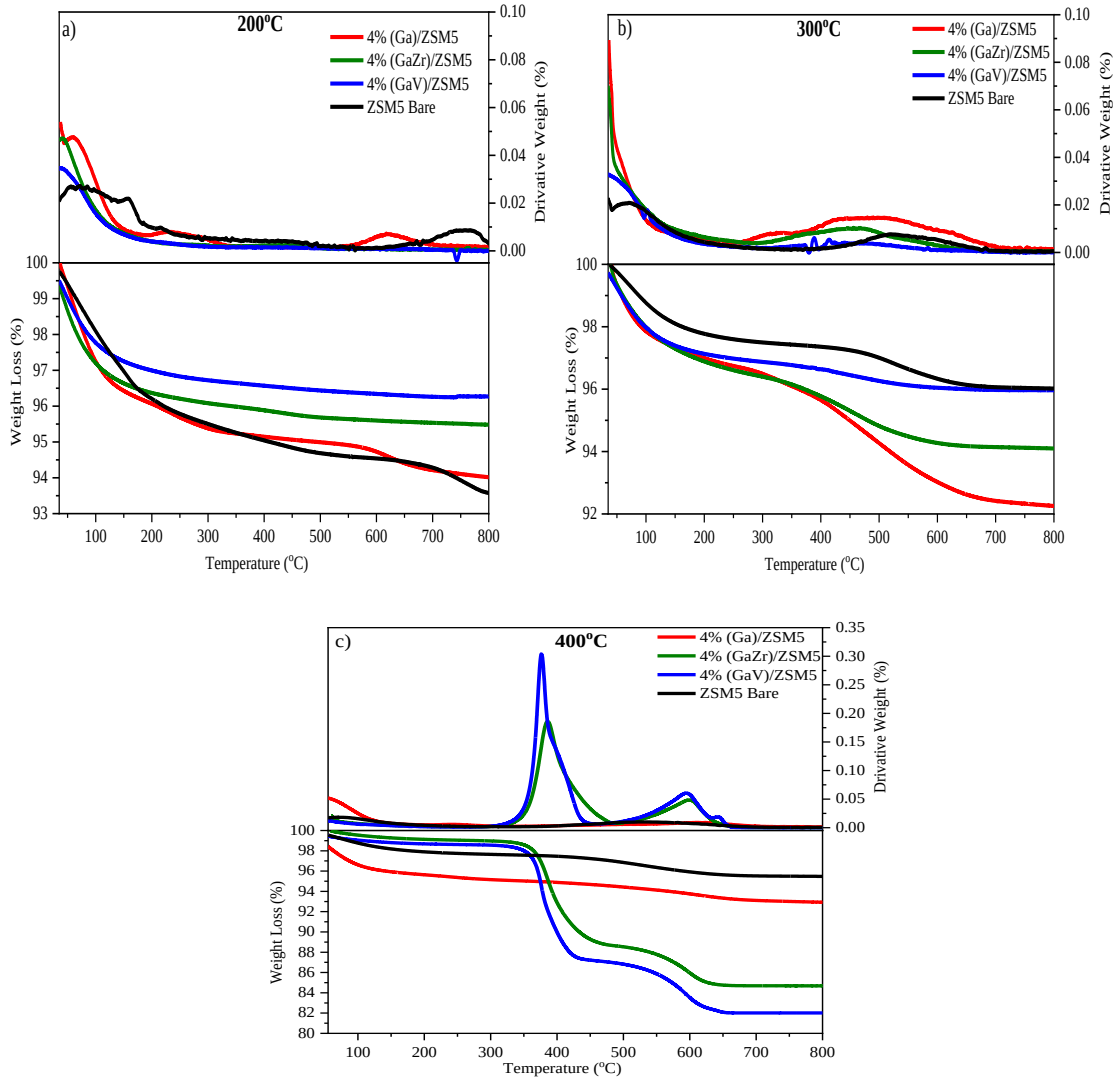

Figure 9. TGA (lower) and DTA (upper) profiles of the spent catalysts after 5 h of MTD at, a) 200°C, b) 300°C, and c) 400°C.

ACKNOWLEDGMENTS

We thank the faculty and staff in the Materials Research Center (MRC) of Missouri S&T for assisting with XRD and SEM-EDX characterization.

REFERENCES

1. Dalena F, Senatore A, Marino A, Gordano A, Basile M, Basile A. Methanol Production and Applications: An Overview. Methanol Sci Eng. 2018; 3–28.

2. Alavi M, Jazayeri-rad H, Behbahani RM. Optimizing the Feed Conditions in a DME Production Process to Maximize the Methanol Conversion. Sci Technol. 2013; 3(2):61–6.

3. Raoof F, Taghizadeh M, Eliassi A, Yaripour F. Effects of temperature and feed composition on catalytic dehydration of methanol to dimethyl ether over γ-alumina. Fuel. 2008; 87(13–14):2967–71.

4. Zhang L, Wang J, Wu P, Hou Z, Fei J, Zheng X. Synthesis of dimethyl ether via methanol dehydration over combined Al2O3-HZSM-5 solid acids. Cuihua Xuebao/Chinese J Catal [Internet]. 2010; 31(8):987–92. Available from: http://dx.doi.org/10.1016/S1872-2067 (10)60098-8

5. Bakhtyari A, Parhoudeh M, Rahimpour MR. Optimal conditions in converting methanol to dimethyl ether, methyl formate, and hydrogen utilizing a double membrane heat exchanger reactor. J Nat Gas Sci Eng [Internet]. 2016; 28:31–45. Available from: http://dx.doi.org/10.1016/j.jngse.2015.11.028

6. Ahlgren S, Baky A, Bernesson S, Nordberg Å, Norén O, Hansson P-A. Future fuel supply systems for organic production based on Fischer–Tropsch diesel and dimethyl ether from on-farm-grown biomass. Biosyst Eng [Internet]. 2008; 99(1):145–55. Available from: http://www.sciencedirect.com/science/article/pii/S1537511007002486

7. Li J-L, Zhang X-G, Inui T. Improvement in the catalyst activity for direct synthesis of dimethyl ether from synthesis gas through enhancing the dispersion of CuO/ZnO/γ-Al2O3 in hybrid catalysts. Appl Catal A Gen [Internet]. 1996; 147(1):23–33. Available from: http://www.sciencedirect.com/science/article/pii/S0926860X96002086

8. SPIVEY JJ. REVIEW: DEHYDRATION CATALYSTS FOR THE METHANOL/DIMETHYL ETHER REACTION. Chem Eng Commun [Internet]. 1991 Dec 1; 110(1):123–42. Available from: https://doi.org/10.1080/00986449108939946

9. Teng H, McCandless JC, Schneyer JB. Thermochemical characteristics of dimethyl ether - An alternative fuel for compression-ignition engines. SAE Tech Pap. 2001 ;(724).

10. Zhu Z, Li DK, Liu J, Wei YJ, Liu SH. Investigation on the regulated and unregulated emissions of a DME engine under different injection timing. Appl Therm Eng [Internet]. 2012; 35:9–14. Available from: http://www.sciencedirect.com/science/article/pii/S1359431111004455

11. Fleisch TH, Basu A, Sills RA. Introduction and advancement of a new clean global fuel: The status of DME developments in China and beyond. J Nat Gas Sci Eng [Internet]. 2012; 9:94–107. Available from: http://dx.doi.org/10.1016/j.jngse.2012.05.012

12. Olah GA, Goeppert A, Prakash GKS. Chemical recycling of carbon dioxide to methanol and dimethyl ether: From greenhouse gas to renewable, environmentally carbon neutral fuels and synthetic hydrocarbons. J Org Chem. 2009; 74(2):487–98.

13. Fleisch TH, Basu A, Gradassi MJ, Masin JG. Dimethyl ether: A fuel for the 21st century. In: de Pontes M, Espinoza RL, Nicolaides CP, Scholtz JH, Scurrell MSBT-S in SS and C, editors. Natural Gas Conversion IV [Internet]. Elsevier; 1997. p. 117–25. Available from: http://www.sciencedirect.com/science/article/pii/S0167299197803230

14. Shikada T, Ohno Y, Ogawa T, Ono M, Mizuguchi M, Tomura K, et al. Direct Synthesis of Dimethyl Ether form Synthesis Gas. In: Parmaliana A, Sanfilippo D, Frusteri F, Vaccari A, Arena FBT-S in SS and C, editors. Natural Gas Conversion V [Internet]. Elsevier; 1998. p. 515–20. Available from: http://www.sciencedirect.com/science/article/pii/S0167299198804837

15. Faungnawakij K, Fukunaga T, Kikuchi R, Eguchi K. Deactivation and regeneration behaviors of copper spinel–alumina composite catalysts in steam reforming of dimethyl ether. J Catal [Internet]. 2008; 256(1):37–44. Available from: http://www.sciencedirect.com/science/article/pii/S002195170800081X

16. Hosseini Z, Taghizadeh M, Yaripour F. Synthesis of nanocrystalline γ-Al2O3 by sol-gel and precipitation methods for methanol dehydration to dimethyl ether. J Nat Gas Chem [Internet]. 2011; 20(2):128–34. Available from: http://www.sciencedirect.com/science/article/pii/S1003995310601727

17. Kim JH, Park MJ, Kim SJ, Joo OS, Jung KD. DME synthesis from synthesis gas on the admixed catalysts of Cu/ZnO/Al 2O3 and ZSM-5. Appl Catal A Gen. 2004; 264file ://(1):37–41.

18. Kim SD, Baek SC, Lee YJ, Jun KW, Kim MJ, Yoo IS. Effect of γ-alumina content on catalytic performance of modified ZSM-5 for dehydration of crude methanol to dimethyl ether. Appl Catal A Gen. 2006; 309(1):139–43.

19. Ha KS, Lee YJ, Bae JW, Kim YW, Woo MH, Kim HS, et al. New reaction pathways and kinetic parameter estimation for methanol dehydration over modified ZSM-5 catalysts. Appl Catal A Gen [Internet]. 2011; 395(1–2):95–106. Available from: http://dx.doi.org/10.1016/j.apcata.2011.01.025

20. Rownaghi AA, Rezaei F, Stante M, Hedlund J. Selective dehydration of methanol to dimethyl ether on ZSM-5 nanocrystals. Appl Catal B Environ [Internet]. 2012; 119–120:56–61. Available from: http://dx.doi.org/10.1016/j.apcatb.2012.02.017

21. Vishwanathan V, Roh HS, Kim JW, Jun KW. Surface properties and catalytic activity of TiO2-ZrO 2 mixed oxides in dehydration of methanol to dimethyl ether. Catal Letters. 2004; 96(1–2):23–8.

22. Jiang S, Hwang JS, Jin T, Cai T, Cho W, Baek YS, et al. Dehydration of Methanol to Dimethyl Ether over ZSM-5 Zeolite. Bull Korean Chem Soc. 2004; 25(2):185–9.

23. Ledesma C, Llorca J. CuZn/ZrO2 catalytic honeycombs for dimethyl ether steam reforming and autothermal reforming. Fuel. 2013; 104:711–6.

24. Magzoub F, Li X, Al-Darwish J, Rezaei F, Rownaghi AA. 3D-printed ZSM-5 monoliths with metal dopants for methanol conversion in the presence and absence of carbon dioxide. Appl Catal B Environ [Internet]. 2019; 245(September 2018):486–95. Available from: https://doi.org/10.1016/j.apcatb.2019.01.008

25. Li X, Kant A, He Y, Thakkar H V, Atanga MA, Rezaei F, et al. Light olefins from renewable resources: Selective catalytic dehydration of bioethanol to propylene over zeolite and transition metal oxide catalysts. Catal Today [Internet]. 2016; 276:62–77. Available from: http://www.sciencedirect.com/science/article/pii/S0920586116300608

26. Jakus AE, Taylor SL, Geisendorfer NR, Dunand DC, Shah RN. Metallic Architectures from 3D-Printed Powder-Based Liquid Inks. Adv Funct Mater. 2015; 25(45):6985–95.

27. Lefevere J, Protasova L, Mullens S, Meynen V. 3D-printing of hierarchical porous ZSM-5: The importance of the binder system. Mater Des [Internet]. 2017; 134:331–41. Available from: http://www.sciencedirect.com/science/article/pii/S0264127517307967

28. Lefevere J, Mullens S, Meynen V. The impact of formulation and 3D-printing on the catalytic. Chem Eng J [Internet]. 2018; 349(November 2017):260–8. Available from: https://doi.org/10.1016/j.cej.2018.05.058

29. Li X, Rezaei F, Rownaghi AA. Methanol-to-olefin conversion on 3D-printed ZSM-5 monolith catalysts: Effects of metal doping, mesoporosity and acid strength. Microporous Mesoporous Mater. 2019; 276(September 2018):1–12.

30. Lawson S, Al-Naddaf Q, Krishnamurthy A, Amour MS, Griffin C, Rownaghi AA, et al. UTSA-16 Growth within 3D-Printed Co-Kaolin Monoliths with High Selectivity for CO2/CH4, CO2/N2, and CO2/H2 Separation. ACS Appl Mater Interfaces. 2018; 10(22):19076–86.

31. Magzoub F, Li X, Lawson S, Rezaei F, Rownaghi AA. 3D-printed HZSM-5 and 3D-HZM5@SAPO-34 structured monoliths with controlled acidity and porosity for conversion of methanol to dimethyl either. Fuel [Internet]. 2020; 280(June):118628. Available from: https://doi.org/10.1016/j.fuel.2020.118628

32. Lawson S, Griffin C, Rapp K, Rownaghi AA, Rezaei F. Amine-Functionalized MIL-101 Monoliths for CO2 Removal from Enclosed Environments. Energy and Fuels. 2019; 33(3):2399–407.

33. Magzoub F, Li X, Lawson S, Rezaei F, Rownaghi AA. 3D-printed HZSM-5 and 3D-HZM5@SAPO-34 structured monoliths with controlled acidity and porosity for conversion of methanol to dimethyl either. Fuel. 2020; 280(June):118628.

34. Farsad A, Lawson S, Rezaei F, Rownaghi AA. Oxidative Dehydrogenation of Propane over 3D Printed Mixed Metal Oxides/H-ZSM-5 Monolithic Catalysts Using CO2 as an Oxidant. Catal Today [Internet]. 2020; Available from: http://www.sciencedirect.com/science/article/pii/S0920586120306738

35. Li X, Rezaei F, Ludlow DK, Rownaghi AA. Synthesis of SAPO-34@ZSM-5 and SAPO-34@Silicalite-1 Core-Shell Zeolite Composites for Ethanol Dehydration. Ind Eng Chem Res. 2018; 57(5):1446–53.

36. Freeman D, Wells RPK, Hutchings GJ. Conversion of methanol to hydrocarbons over Ga2O3/H-ZSM-5 and Ga2O3/WO3 catalysts. J Catal. 2002; 205(2):358–65.

37. Shao T, Zhang P, Jin L, Li Z. Photocatalytic decomposition of perfluorooctanoic acid in pure water and sewage water by nanostructured gallium oxide. Appl Catal B Environ. 2013; 142–143:654–61.

38. Matmin J. Rice Starch-Templated Synthesis of Nanostructured. Proceedings. 2019; 3(1):3–7.

39. Näfe H, Karpukhina N. Na-modified cubic zirconia - Link between sodium zirconate and zirconia in the Na2O-ZrO2 phase diagram. J Am Ceram Soc. 2007; 90(5):1597–602.

40. Petráš M, Wichterlová B. High-temperature interaction of vanadium pentoxide with H-ZSM-5 zeolite. ESR and IR study. J Phys Chem. 1992; 96(4):1805–9.

41. Nesamani IFP, Prabha VL, Paul A, Nirmal D. Synthesis and dielectric studies of monoclinic nanosized zirconia. Adv Condens Matter Phys. 2014; 2014.

42. Thommes M, Kaneko K, Neimark A V., Olivier JP, Rodriguez-Reinoso F, Rouquerol J, et al. Physisorption of gases, with special reference to the evaluation of surface area and pore size distribution (IUPAC Technical Report). Pure Appl Chem. 2015; 87(9–10):1051–69.

43. Lawson S, Adebayo B, Robinson C, Al-Naddaf Q, Rownaghi AA, Rezaei F. The effects of cell density and intrinsic porosity on structural properties and adsorption kinetics in 3D-printed zeolite monoliths. Chem Eng Sci [Internet]. 2020; 218:115564. Available from: https://doi.org/10.1016/j.ces.2020.115564

44. Id CREF, Umr ML, Library M. xxx.

45. Moreno JA, Poncelet G. Isomerization of n-butane over sulfated Al- and Ga-promoted zirconium oxide catalysts. Influence of promoter and preparation method. J Catal. 2001; 203(2):453–65.

46. Štefanić G, Musić S. Thermal behavior of the amorphous precursors of the ZrO2-GaO1.5 system. J Alloys Compd. 2008; 460(1–2):444–52.

47. Liu X, Zhong S, Yang F, Su H, Lin W, Chen J, et al. Template-Free Synthesis of High-Content Vanadium-Doped ZSM-5 with Enhanced Catalytic Performance. ChemistrySelect. 2017; 2(35):11513–20.

48. Duin JJB Van. Aromatization of Ketones over Zeolite Catalysts. 2018 ;(March).

49. Koranne MM, Goodwin JG, Marcelin G. Characterization of Silica- and Alumina-Supported Vanadia Catalysts Using Temperature Programmed Reduction. J Catal. 1994; 148(1):369–77.

50. Chary KVR, Kishan G, Kumar CP, Sagar GV. Structure and catalytic properties of vanadium oxide supported on alumina. Appl Catal A Gen. 2003; 246(2):335–50.

51. Juybar M, Kanmohammadi Khorrami M, Bagheri Garmarudi A. Conversion of methanol to aromatics over ZSM-5/11 intergrowth Zeolites and bimetallic Zn-Cu-ZSM-5/11 and Ga-Ag-ZSM-5/11 catalysts prepared with direct synthesis method. J Chem Sci [Internet]. 2019; 131(10):1–14. Available from: https://doi.org/10.1007/s12039-019-1684-8

52. Xu L, Wu S, Guan J, Wang H, Ma Y, Song K, et al. Synthesis, characterization of hierarchical ZSM-5 zeolite catalyst and its catalytic performance for phenol tert-butylation reaction. Catal Commun. 2008; 9(6):1272–6.

53. Veses A, Puértolas B, Callén MS, García T. Catalytic upgrading of biomass derived pyrolysis vapors over metal-loaded ZSM-5 zeolites: Effect of different metal cations on the bio-oil final properties. Microporous Mesoporous Mater. 2015; 209:189–96.

54. Chen W-H, Ko H-H, Sakthivel A, Huang S-J, Liu S-H, Lo A-Y, et al. A solid-state NMR, FT-IR and TPD study on acid properties of sulfated and metal-promoted zirconia: Influence of promoter and sulfation treatment. Catal Today. 2006; 116(2):111–20.

55. Llorca J, Homs N, Sales J, Ramírez De La Piscina P. Support effect on the n-hexane dehydrogenation reaction over platinum-tin catalysts. Stud Surf Sci Catal. 1998; 119:647–52.

SECTION

2. CONCLUSIONS AND FUTURE WORK

2.1. CONCLUSIONS

In this dissertation, multiple zeolite catalysts were designed out of 3D-printing monoliths to create fine-tuning micro-meso-macro-porosity and structured the surface acidity by incorporating several metal oxides via different methods. The designed and structured zeolites were used in methanol conversion as heterogeneous catalysts to produced hydrocarbons and through a catalyzed methanol dehydration to form dimethyl ether.

In brief detail, the zeolite monoliths were modified by adding metal precursor into the preparation paste step before the 3D printing process. A group of 3D-printed zeolite doped with Ga_2O_3, Cr_2O_3, CuO, ZnO, MoO_3, and Y_2O_3 was synthesized. The influence of metal dopants in the 3D-printed ZSM-5 monolith catalysts for the methanol to hydrocarbons (MTH) reaction was investigated in the presence and absence of CO_2 and their performance evaluation was tested in a fixed-bed reactor. No promotional effect after dopping with metals on the MFI framework of ZSM5 but the porosity and the acidity of the catalysts were changed. That Y- and Zn-doped ZSM-5 monoliths exhibited higher yield of light olefins and BTX compounds in the absence and presence of CO_2, respectively

Furthermore, the utilization of the 3D printing technique method for manufacturing catalytic catalysts was investigated. This fabrication method provides quick and simple steps, low financially, and an easy way of making customized structured catalysts. 3D-

printed HZSM-5 zeolite was successfully synthesized, and the HSZM5 monoliths were followed by coated with SAPO-34 layers. The HZSM5 monolith and its counterpart power has been compared about their surface area and porosity. Also, the 3D-printing monolith design affected the zeolite acidity. Generally, the catalyst properties confirmed the stability of the HZSM-5 catalyst in methanol dehydration and enhanced the production of DME. Additional, 3D HZSM5@SAPO-34 structured monolith promoted the density of strong acid sites led to form higher hydrocarbons.

Moreover, the small load percentage weight of Ga, Zr, and V incorporates with HZSM5 and is designed as 3D-printing monoliths and test their behaver in Methanol to DME to evaluate the stability and selectivity toward DME formation. All the monolith achieved high conversion at low temperature but Ga as a monometallic monolith enhance the production of DME. On the other side, the increase in the reaction temperature boost to form of other hydrocarbons.

2.2. FUTURE WORK

For designed and manufactured as a 3D-printing monolith, influenced many factors such as the thickness of the wall, channel dimensions and shape, and the number of layers, could be improved, for better achievement and performance and to develop the 3D-printing technique. Besides the coating method in zeolites has been reported in different processes but the effect of the coating thickness as a parameter must be studied. Also, the study of the effect of monometallic, bimetallic, and mixmetalic oxides incorporated with ZSM5 in a 3D-printing monolith, in the structure and characterization could go into deep

investigation. Besides the effect of the metal loading could be counted as an important parameter in all heterogeneous catalysts.

Also, direct synthesis of DME from synthesis gas ($CO+H_2$) can be investigated on bifunctional catalysts, containing $CuZnO/Al_2O_3$ and ZSM-5 promoted with Zr or Ga on V as a methanol dehydration catalyst.

BIBLIOGRAPHY

1. Dyer A. Zeolites. In: Buschow KHJ, Cahn RW, Flemings MC, et al., eds. Oxford: Elsevier; 2001:9859-9863. doi:https://doi.org/10.1016/B0-08-043152-6/01784-8

2. Boyd GE, Schubert J, Adamson AW. The Exchange Adsorption of Ions from Aqueous Solutions by Organic Zeolites. Ion-exchange Equilibria. *J Am Chem Soc*. 1947;69(11):2818-2829. doi:10.1021/ja01203a064

3. Ríos CA, Williams CD, Fullen MA. Nucleation and growth history of zeolite LTA synthesized from kaolinite by two different methods. *Appl Clay Sci*. 2009;42(3):446-454. doi:https://doi.org/10.1016/j.clay.2008.05.006

4. Pavelić SK, Medica JS, Gumbarević D, Filošević A, Pržulj N, Pavelić K. Critical review on zeolite clinoptilolite safety and medical applications in vivo. *Front Pharmacol*. 2018;9(NOV):1-15. doi:10.3389/fphar.2018.01350

5. Online. Zeolite structre.

6. Shih W-H, Chang H-L. Conversion of fly ash into zeolites for ion-exchange applications. *Mater Lett*. 1996;28(4):263-268. doi:https://doi.org/10.1016/0167-577X(96)00064-X

7. Zhang J, Singh R, Webley PA. Alkali and alkaline-earth cation exchanged chabazite zeolites for adsorption based CO2 capture. *Microporous Mesoporous Mater*. 2008;111(1):478-487. doi:https://doi.org/10.1016/j.micromeso.2007.08.022

8. Jiang N, Shang R, Heijman SGJ, Rietveld LC. High-silica zeolites for adsorption of organic micro-pollutants in water treatment: A review. *Water Res*. 2018;144:145-161. doi:https://doi.org/10.1016/j.watres.2018.07.017

9. Auerbach S, Carrado K, Dutta P, Sircar S, Myers A. Gas Separation by Zeolites. *Handb Zeolite Sci Technol*. 2003. doi:10.1201/9780203911167.ch22

10. Novotný J, Reichel P, Bárdová K, Kyzeková P, Almášiová V. The Effects of Clinoptilolite Administration on the Appetite, the Consistency of Faeces and the Histology of the Small Intestine in Growing Pigs. *Folia Vet*. 2019;63(3):47-52. doi:10.2478/fv-2019-0026

11. Abbasian S, Taghizadeh M. Preparation of H-ZSM-5 Nano-Zeolite Using Mixed Template Method and its Activity Evaluation for Methanol to DME Reaction. *Int J Nanosci Nanotechnol*. 2014;10(3):171-180.

12. Yarulina I, Kapteijn F, Gascon J. The importance of heat effects in the methanol to hydrocarbons reaction over ZSM-5: On the role of mesoporosity on catalyst performance. *Catal Sci Technol*. 2016;6(14):5320-5325. doi:10.1039/c6cy00654j

13. Olsbye U, Svelle S, Bjrgen M, et al. Conversion of methanol to hydrocarbons: How zeolite cavity and pore size controls product selectivity. *Angew Chemie - Int Ed*. 2012;51(24):5810-5831. doi:10.1002/anie.201103657

14. Wang T, Tang X, Huang X, et al. Conversion of methanol to aromatics in fluidized bed reactor. *Catal Today*. 2014;233:8-13. doi:10.1016/j.cattod.2014.02.007

15. Tian P, Wei Y, Ye M, Liu Z. Methanol to olefins (MTO): From fundamentals to commercialization. *ACS Catal*. 2015;5(3):1922-1938. doi:10.1021/acscatal.5b00007

16. Li J, Wei Y, Liu G, et al. Comparative study of MTO conversion over SAPO-34, H-ZSM-5 and H-ZSM-22: Correlating catalytic performancfile:///C:/Users/fmzp5/Downloads/cs3006583.pdfe and reaction mechanism to zeolite topology. *Catal Today*. 2011;171(1):221-228. doi:10.1016/j.cattod.2011.02.027

17. Ilias S, Bhan A. Mechanism of the catalytic conversion of methanol to hydrocarbons. *ACS Catal*. 2013;3(1):18-31. doi:10.1021/cs3006583

18. Bjørgen M, Svelle S, Joensen F, et al. Conversion of methanol to hydrocarbons over zeolite H-ZSM-5: On the origin of the olefinic species. *J Catal*. 2007;249(2):195-207. doi:10.1016/j.jcat.2007.04.006

19. Lefevere J, Mullens S, Meynen V, Van Noyen J. Structured catalysts for methanol-to-olefins conversion: A review. *Chem Pap*. 2014;68(9):1143-1153. doi:10.2478/s11696-014-0568-0

20. Zhang C, Jun KW, Kwak G, Kim S. Energy-Efficient Methanol to Dimethyl Ether Processes Combined with Water-Containing Methanol Recycling: Process Simulation and Energy Analysis. *Energy Technol*. 2019;7(1):167-176. doi:10.1002/ente.201800469

21. Masih D, Rohani S, Kondo JN, Tatsumi T. Low-temperature methanol dehydration to dimethyl ether over various small-pore zeolites. *Appl Catal B Environ*. 2017;217:247-255. doi:10.1016/j.apcatb.2017.05.089

22. Al-Fatesh ASA, Fakeeha AH, Abasaeed AE. Effects of selected promoters on Ni/Y-Al 2O 3 catalyst performance in methane dry reforming. *Chinese J Catal*. 2011;32(9-10):1604-1609. doi:10.1016/S1872-2067(10)60267-7

23. Catizzone E, Aloise A, Migliori M, Giordano G. Dimethyl ether synthesis via methanol dehydration: Effect of zeolite structure. *Appl Catal A Gen*. 2015;502:215-220. doi:10.1016/j.apcata.2015.06.017

24. Parra-Cabrera C, Achille C, Kuhn S, Ameloot R. 3D printing in chemical engineering and catalytic technology: Structured catalysts, mixers and reactors. *Chem Soc Rev*. 2018;47(1):209-230. doi:10.1039/c7cs00631d

25. Lind A, Vistad Ø, Sunding MF, Andreassen KA, Cavka JH, Grande CA. Multi-purpose structured catalysts designed and manufactured by 3D printing. *Mater Des*. 2020;187:1-8. doi:10.1016/j.matdes.2019.108377

26. Thakkar H, Eastman S, Hajari A, Rownaghi AA, Knox JC, Rezaei F. 3D-Printed Zeolite Monoliths for CO2 Removal from Enclosed Environments. *ACS Appl Mater Interfaces*. 2016;8(41):27753-27761. doi:10.1021/acsami.6b09647

27. Lawson S, Al-Naddaf Q, Krishnamurthy A, et al. UTSA-16 Growth within 3D-Printed Co-Kaolin Monoliths with High Selectivity for CO2/CH4, CO2/N2, and CO2/H2 Separation. *ACS Appl Mater Interfaces*. 2018;10(22):19076-19086. doi:10.1021/acsami.8b05192

28. Thakkar H, Lawson S, Rownaghi AA, Rezaei F. Development of 3D-printed polymer-zeolite composite monoliths for gas separation. *Chem Eng J*. 2018;348:109-116. doi:https://doi.org/10.1016/j.cej.2018.04.178

29. Couck S, Cousin-Saint-Remi J, Van der Perre S, et al. 3D-printed SAPO-34 monoliths for gas separation. *Microporous Mesoporous Mater*. 2018;255:185-191. doi:https://doi.org/10.1016/j.micromeso.2017.07.014

30. Thakkar H, Eastman S, Al-Mamoori A, Hajari A, Rownaghi AA, Rezaei F. Formulation of Aminosilica Adsorbents into 3D-Printed Monoliths and Evaluation of Their CO2 Capture Performance. *ACS Appl Mater Interfaces*. 2017;9(8):7489-7498. doi:10.1021/acsami.6b16732

31. Thakkar H, Eastman S, Al-Naddaf Q, Rownaghi AA, Rezaei F. 3D-Printed Metal-Organic Framework Monoliths for Gas Adsorption Processes. *ACS Appl Mater Interfaces*. 2017;9(41):35908-35916. doi:10.1021/acsami.7b11626

32. Lv G, Bin F, Song C, Wang K, Song J. Promoting effect of zirconium doping on Mn/ZSM-5 for the selective catalytic reduction of NO with NH3. *Fuel*. 2013;107(x):217-224. doi:10.1016/j.fuel.2013.01.050

33. Rahmani F, Haghighi M, Vafaeian Y, Estifaee P. Hydrogen production via CO2 reforming of methane over ZrO2-Doped Ni/ZSM-5 nanostructured catalyst prepared by ultrasound assisted sequential impregnation method. *J Power Sources*. 2014;272:816-827. doi:10.1016/j.jpowsour.2014.08.123

34. Ates A, Hardacre C. The effect of various treatment conditions on natural zeolites: Ion exchange, acidic, thermal and steam treatments. *J Colloid Interface Sci*. 2012;372(1):130-140. doi:10.1016/j.jcis.2012.01.017

35. Veses A, Puértolas B, Callén MS, García T. Catalytic upgrading of biomass derived pyrolysis vapors over metal-loaded ZSM-5 zeolites: Effect of different metal cations on the bio-oil final properties. *Microporous Mesoporous Mater*. 2015;209:189-196. doi:https://doi.org/10.1016/j.micromeso.2015.01.012

VITA

Fatima Mahgoub Magzoub was born in PortSudan, Sudan. She started her studies in Chemical Engineering and Technology at Red Sea University of Chemical Engineering, Sudan, in September 2006 and received a Bachelor of Science in Chemical Engineering in May 2010. She enrolled in the Missouri University of Science and Technology for her graduate studies in 2015 and received a Master of Science degree in Chemical Engineering in December 2016. In 2017, she started her research and studies at the Department of Chemical and Biochemical Engineering of Missouri University of Science and Technology, in Rolla, Missouri. She received the Doctor of Philosophy in Chemical Engineering from Missouri University of Science and Technology in December 2020.